Estimation of fossil-fuel CO2 emissions using satellite measurements of "proxy" species

Igor B. Konovalov, Evgeny V. Berezin, Philippe Ciais, Grégoire Broquet, Ruslan V. Zhuravlev, Greet Janssens-Maenhout

Atmos. Chem. Phys., 16, 13509–13540, 2016
www.atmos-chem-phys.net/16/13509/2016/
doi:10.5194/acp-16-13509-2016

Atmospheric Chemistry and Physics Open Access EGU

Estimation of fossil-fuel CO_2 emissions using satellite measurements of "proxy" species

Igor B. Konovalov[1], Evgeny V. Berezin[1], Philippe Ciais[2], Grégoire Broquet[2], Ruslan V. Zhuravlev[1], and Greet Janssens-Maenhout[3]

[1]Institute of Applied Physics, Russian Academy of Sciences, Nizhniy Novgorod, Russia
[2]Laboratoire des Sciences du Climat et l'Environnement (LSCE/IPSL), CNRS-CEA-UVSQ, Centre d'Études Orme des Merisiers, Gif-sur-Yvette, France
[3]Joint Research Center, Institute for Environment and Sustainability, Ispra (Va), Italy

Correspondence to: Igor B. Konovalov (konov@appl.sci-nnov.ru)

Received: 13 April 2016 – Published in Atmos. Chem. Phys. Discuss.: 19 April 2016
Revised: 24 September 2016 – Accepted: 13 October 2016 – Published: 1 November 2016

Abstract. Fossil-fuel (FF) burning releases carbon dioxide (CO_2) together with many other chemical species, some of which, such as nitrogen dioxide (NO_2) and carbon monoxide (CO), are routinely monitored from space. This study examines the feasibility of estimation of FF CO_2 emissions from large industrial regions by using NO_2 and CO column retrievals from satellite measurements in combination with simulations by a mesoscale chemistry transport model (CTM). To this end, an inverse modeling method is developed that allows estimating FF CO_2 emissions from different sectors of the economy, as well as the total CO_2 emissions, in a given region. The key steps of the method are (1) inferring "top-down" estimates of the regional budget of anthropogenic NO_x and CO emissions from satellite measurements of proxy species (NO_2 and CO in the case considered) without using formal a priori constraints on these budgets, (2) the application of emission factors (the NO_x-to-CO_2 and CO-to-CO_2 emission ratios in each sector) that relate FF CO_2 emissions to the proxy species emissions and are evaluated by using data of "bottom-up" emission inventories, and (3) cross-validation and optimal combination of the estimates of CO_2 emission budgets derived from measurements of the different proxy species. Uncertainties in the top-down estimates of the NO_x and CO emissions are evaluated and systematic differences between the measured and simulated data are taken into account by using original robust techniques validated with synthetic data. To examine the potential of the method, it was applied to the budget of emissions for a western European region including 12 countries by using NO_2 and CO column amounts retrieved from, respectively, the OMI and IASI satellite measurements and simulated by the CHIMERE mesoscale CTM, along with the emission conversion factors based on the EDGAR v4.2 emission inventory. The analysis was focused on evaluation of the uncertainty levels for the top-down NO_x and CO emission estimates and "hybrid" estimates (that is, those based on both atmospheric measurements of a given proxy species and respective bottom-up emission inventory data) of FF CO_2 emissions, as well as on examining consistency between the FF NO_2 emission estimates derived from measurements of the different proxy species. It is found that NO_2 measurements can provide much stronger constraints to the total annual FF CO_2 emissions in the study region than CO measurements, the accuracy of the NO_2-measurement-based CO_2 emission estimate being mostly limited by the uncertainty in the top-down NO_x emission estimate. Nonetheless, CO measurements are also found to be useful as they provide additional constraints to CO_2 emissions and enable evaluation of the hybrid FF CO_2 emission estimates obtained from NO_2 measurements. Our most reliable estimate for the total annual FF CO_2 emissions in the study region in 2008 (2.71 ± 0.30 Pg CO_2) is found to be about 11 and 5 % lower than the respective estimates based on the EDGAR v.4.2 (3.03 Pg CO_2) and CDIAC (2.86 Pg CO_2) emission inventories, with the difference between our estimate and the CDIAC inventory data not being statistically significant. In general, the results of this study indicate that the proposed method has the potential to become a useful tool for identification of pos-

sible biases and/or inconsistencies in the bottom-up emission inventory data regarding CO_2, NO_x, and CO emissions from fossil-fuel burning in different regions of the world.

1 Introduction

Carbon dioxide (CO_2) is commonly recognized as the major greenhouse gas providing the driving force of recent and future climate change (IPCC, 2013). Its atmospheric concentration has considerably increased (by 40 %) since the industrial revolution (Petit et al., 1999). This increase, the rate of which has accelerated in the past decade, is attributed mostly to anthropogenic sources, such as fossil-fuel (FF) burning (Canadell et al., 2007). Curbing further growth of CO_2 concentration has become a goal of international agreements such as the Kyoto protocol (UNFCCC, 1998) and the Paris Agreement on Climate Change (UNFCCC, 2015). Thus accurate knowledge of anthropogenic CO_2 emissions is of paramount importance both for climate prediction and mitigation policy purposes.

Over the past few decades a lot of effort has been put into the compilation of global (e.g., Olivier et al., 2005; GCP, 2010; Ciais et al., 2010a; Janssens-Maenhout et al., 2015) as well as regional (Gurney et al., 2009; Huang et al., 2011; Kurokawa et al., 2013; Zhao et al., 2012; Wang et al., 2013) inventories of CO_2 emissions from FF burning and other smaller anthropogenic sources (such as biofuel burning and cement production). Those emission inventories are based on available statistical information regarding economic activities and corresponding technologies. However, it is known that such information can be subject to errors and biases leading to considerable uncertainties in emission estimates, especially in the case of rapidly growing developing economies (e.g., Akimoto et al., 2006; Guan et al., 2012; Korsbakken et al., 2016). For example, the uncertainty of available estimates of the total FF CO_2 emissions in China is assessed to be about 15–20 % (Gregg et al., 2008). Much larger uncertainties may be associated with the subnational spatial distributions and temporal evolution of FF CO_2 emissions within a year (Ciais et al., 2010b). The uncertainties in anthropogenic CO_2 emission inventory data are mostly due to inaccuracies of available data regarding fuel consumption and fuel chemical composition. Note that the estimation of uncertainty in emission inventory data is itself a challenging task: in particular, as different inventories are usually based (at least partly) on common sources of information, their intercomparison does not necessarily result in revealing all the uncertainties.

A promising alternative approach to constrain NO_2 emissions and to assess the uncertainty in available emission estimates is inverse modeling (Enting, 2002); the key idea of this approach is to derive emission estimates from atmospheric measurement data by optimizing emissions coupled to a transport model. Such estimates are frequently referred to as "top-down", in contrast to "bottom-up" ones based on emission inventories alone. Numerous studies have successfully used in situ CO_2 measurements in the framework of this approach to constrain surface CO_2 fluxes associated mostly with biospheric and oceanic sources and sinks of CO_2 in different regions of the world (e.g., Gurney et al., 2002; Baker et al., 2006; Schulze et al., 2009; Chevallier et al., 2010; Broquet et al., 2013). More recently, it was demonstrated that uncertainties in CO_2 flux estimates can be potentially reduced by using satellite CO_2 measurements (e.g., Chevallier et al., 2007; Houweling et al., 2004; Hungershoefer et al., 2010; Kadygrov et al., 2009; Nassar et al., 2011; Maksyutov et al., 2013; Reuter et al., 2014a). However, less progress has been made in isolating FF CO_2 emissions from other sources and sinks. Major limitations are due to the fact that the atmospheric variability of CO_2 is strongly affected by biogenic sources and sinks, such as plant respiration and photosynthesis, and that the signatures of regional FF CO_2 emissions in CO_2 observations are typically weak relative to regional background CO_2 concentration, except near hot spots. Promising approaches suggest separation of FF CO_2 emissions from biospheric fluxes by using available measurements of radiocarbon content (14C) of CO_2 (e.g., Turnbull et al., 2009; Miller et al., 2012; Lehman et al., 2013; Basu et al., 2016), ground-based CO_2 measurements in vicinity of strong anthropogenic emission sources like megacities (Bréon et al., 2015), or satellite CO_2 retrievals with sampling near hotspots (Bovensmann et al., 2010; Silva et al., 2013; Reuter et al., 2014b). However, neither of these approaches has already been sufficiently generalized to provide reliable estimates of the budget of anthropogenic CO_2 emissions in an arbitrary industrialized region of the world.

It has also been suggested that anthropogenic CO_2 emissions can be constrained to a certain extent by measurements of "proxy" species, whose sources are mostly collocated in time and space with CO_2 sources (Rivier et al., 2006; Suntharalingam et al., 2004). The measurements of proxy species can be either combined with CO_2 measurements (Palmer et al., 2006; Rivier et al., 2006; Suntharalingam et al., 2004; Brioude et al., 2012) or used alone but with information on a relationship between emissions of CO_2 and of the proxy species from bottom-up emission inventories. In the second approach, Berezin et al. (2013) estimated multiannual relative changes of FF CO_2 emissions from China by using satellite measurements of nitrogen dioxide (NO_2) and emission inventory data on the ratio of FF emissions of CO_2 and nitrogen oxides ($NO_x = NO + NO_2$). A similar approach was employed by Konovalov et al. (2014) to obtain estimates of CO_2 emissions from biomass burning in Siberia by using satellite measurements of carbon monoxide (CO) and of aerosol optical depth.

The goal of this study is to examine the feasibility of inferring estimates of annual budgets of CO_2 emissions from FF burning in a given industrialized region with a typical size of the order of 1000 km by using satellite measurements of NO_2

and CO. In doing so, we develop a special method by building upon the ideas that were exploited in Berezin et al. (2013) and Konovalov et al. (2014). The method includes several major steps, namely (1) inferring top-down estimates of total anthropogenic emissions of NO_x and CO from satellite measurements of the corresponding proxy species by using simulations performed with a mesoscale chemistry transport model (CTM), (2) applying NO_x-to-CO_2 (or CO-to-CO_2) emission conversion factors given by bottom-up emission inventories to relate FF CO_2 emissions to the NO_x and CO anthropogenic emissions from the previous step, and (3) cross-validation and optimal combination of estimates of the FF CO_2 emission budgets derived from measurements of different proxy species. As a result, we obtain a "hybrid" FF CO_2 emission estimate integrating information coming from measurements and bottom-up inventories. The use of NO_2 and CO as proxy species in the context of our approach is justified because their satellite measurements are known to contain a strong signal associated with human activities in industrial regions and have abundantly been used earlier to constrain emissions of, respectively, NO_x (e.g., Martin et al., 2003; Konovalov et al., 2006; Napelenok et al., 2008; Miyazaki et al., 2012; Gu et al., 2014) and CO (e.g., Arellano et al., 2004; Pétron et al., 2004; Kopacz et al., 2010; Hooghiemstra et al., 2012; Krol et al., 2013; Jiang et al., 2015) from various sources, including anthropogenic ones. Note that although NO_x and CO emissions from FF burning are more sensitive to technological factors than CO_2 emissions, different aspects of the combustion technology are expected to affect NO_x and CO emissions in different ways: e.g., while NO_x emissions are strongly dependent on the temperature of combustion (more NO_x is released at higher temperatures), CO emissions can be regarded as a measure of the incompleteness of combustion processes. So, the combination of hybrid FF CO_2 emission estimates derived from both NO_2 and CO measurements can enable a compensation of a part of the uncertainties associated with inaccurate knowledge of technology and conditions of combustion affecting separately NO_2 and CO measurement based FF CO_2 emission estimates.

Particular efforts in this study were made to provide adequate confidence intervals for the hybrid FF CO_2 emission estimates. To this end, we had to ensure that potential errors in our top-down estimates of NO_x and CO emissions are statistically independent from those of the conversion factors. We also had to ensure that the evaluation of confidence intervals does not involve any subjective quantitative assumptions regarding the level of uncertainties in measured and simulated data. Such requirements would be difficult to satisfy if the top-down estimates of the emission annual budgets were partly constrained (in the Bayesian sense) with a priori knowledge on these budgets from a bottom-up emission inventory (as it is usual in inverse modeling studies). Furthermore, the use of a priori constraints would make the cross-validation of the estimates of FF CO_2 emission budgets based on NO_2 and CO measurements infeasible, as both priors and cross-validation estimates could then be biased in a similar way due to possible systematic uncertainties in activity data employed in the emission inventory. Accordingly, a distinctive feature of our method is that it does not involve any formal a priori constraints to the top-down estimates of the emission budgets or any quantitative settings specifying the level of uncertainties in measured and simulated data. This feature is expected to reinforce the potential of the method to elucidate possible uncertainties and/or inconsistencies in CO_2, NO_x, and CO emission data provided by different bottom-up emission inventories.

In this study, our method is applied for estimation of annual FF CO_2 emissions from a group of 12 western European countries, including a selection of 11 member states of the European Union (EU) that provide the predominant part (> 70 %) of EU total FF carbon emissions (Ciais et al., 2010b) and Switzerland. Taking into account availability of bottom-up emission inventory data necessary for our analysis, the annual emission estimates were obtained specifically for the year 2008. We believe that estimation of FF CO_2 emissions from the European region could be considered as a good testing case for our method, taking into account that uncertainties in corresponding emission inventory data for the EU countries with well-developed statistics are relatively low (compared to potential uncertainties in FF CO_2 emission data for countries with less developed statistical infrastructure), although not quite negligible. For example, by comparing data of several international emission inventories, Ciais et al. (2010b) estimated the full uncertainty of the bottom-up estimates of the anthropogenic CO_2 emissions in the EU countries to be about 19 % but less ($\sim$ 7 %) if possible inconsistencies between types of CO_2 sources are taken into account in different emission inventories are resolved. Note that the uncertainty in bottom-up FF CO_2 emission estimates is expected to be lower than in corresponding NO_x and CO emission estimates because of an important role played for emissions of those proxy species by the technology and end-of-pipe measures; at the same time, the ratio of emissions of CO_2 and of the proxy species can be less uncertain than the emission themselves if the emission data are subject to a strong common bias caused by uncertainties in fuel consumption statistics.

In the following, Sect. 2 describes data and modeling tools used in our study. Description of our inverse modeling method and its validation with synthetic "observations" are presented in Sect. 3. The results of its application to the real-world situation are presented and discussed in Sect. 4. Finally, major findings are summarized in Sect. 5.

2 Data and model description

2.1 Retrievals from satellite measurements

We used the tropospheric NO_2 column retrievals from measurements of the Earth's backscattered radiation in visible and ultraviolet spectral regions by the OMI satellite instrument (Levelt et al., 2006) on board the NASA EOS Aura spacecraft. The Aura satellite (Schoeberl et al., 2006) is in a sun-synchronous ascending polar orbit with an Equator crossing time of 13:30 local solar time (LST) and an orbital period of 99 min. The OMI instrument has a swath width of ~ 2600 km divided into 60 pixels with a size of 13–26 km.

The retrievals used in this study are provided by the Royal Netherlands Meteorological Institute (KNMI) as the DOMINO version 2 data product (Boersma et al., 2011) through the TEMIS portal (http://www.temis.nl/). The product contains Level 2 data, that is, NO_2 columns and relevant geophysical information for each ground pixel observed by the instrument. In this study, only cloud and surface albedo screened data (retrieved for the scenes with the cloud fraction less than 30 % and with the surface albedo less than 0.3) were used. The main steps of the OMI NO_2 retrieval algorithm (see Boersma et al., 2011, for details) include (1) spectral fitting and the slant column density (SCD) estimation by using the differential optical absorption spectroscopy (DOAS) method, (2) separation of the tropospheric and stratospheric parts of the slant columns, and (3) calculation of the tropospheric vertical column by applying the air mass factor (AMF) to the tropospheric slant column. Each step involves different uncertainties that may contribute, to various extents, to the uncertainty of the tropospheric NO_2 columns; in particular, the SCD uncertainty is likely to predominate over other uncertainties in remote areas and is about 0.7×10^{15} molec. cm^{-2}, while the retrievals for urban areas are mostly affected by the AMF uncertainty, that is of about 25 % for cloud-free conditions (Boersma et al., 2007, 2011). Several studies (e.g., Zhao and Wang, 2009; Miyazaki et al., 2012; Vinken et al., 2014) found that in spite of the considerable uncertainties, the tropospheric NO_2 columns retrieved from the OMI measurements provide useful constraints to anthropogenic NO_x emissions in different regions of the world, including Europe.

We also used the Level 2 retrievals of total CO column amounts from the measurements performed by the Infrared Atmospheric Sounding Interferometer (IASI) on board the Metop-A satellite (Clerbaux et al., 2009). Metop-A has the sun-synchronous polar orbit with Equator crossing at 21:30 LST for the ascending node. The IASI instrument provides global coverage twice a day (around 09:30 and 21:30 LST), with a swath of about 2×1100 km and a nominal pixel diameter footprint on the ground of 12 km.

The CO column amounts are retrieved from the cloud screened measurements of the spectrum at the 1–0 rotation vibration band centered at 4.7 µm (2128 cm^{-1}) by using the Fast Optimal Retrievals on Layers for IASI (FORLI) algorithm (Hurtmans et al., 2012). The FORLI algorithm provides CO partial column amounts (for at most 19 layers) fitting the spectral observations with a priori constraints; the partial columns are combined to yield the total column amounts. The uncertainty of the IASI CO retrievals strongly depends on the geographical location and conditions of the observations (Clerbaux et al., 2009; George et al., 2009; Turquety et al., 2009); it is estimated to be about 10 % under typical conditions (Clerbaux et al., 2009). It should be noted, however, that the capability of the IASI measurements to inform about CO sources depends not only on the accuracy of the CO retrievals but also on the sensitivity of the spectral observations to the CO concentration in the boundary layer. A convenient way to characterize this sensitivity (which is related to the vertical resolution of the retrieval and depends, in particular, on the difference between the temperatures of the surface and of the atmospheric boundary layer) is to consider the trace of the averaging kernel matrix (Clerbaux et al., 2009); this parameter is called the degree of freedom of the signal (DOFS). Distinguishing between the upper and lower troposphere requires this parameter to be about 2 (George et al., 2009). Taking these considerations into account, we used only those retrievals that were characterized by relatively large DOFS values: similar to Konovalov et al. (2014), the DOFS threshold was set to be 1.7. The available CO retrievals for individual pixels were projected to the $0.5° \times 0.5°$ grid of a CTM (see Sect. 2.2) and averaged over each day.

We would like to note that instead of (or together with) the IASI measurements, we had an option of using alternative data from other infrared sounders, such as MOPITT and AIRS. Our decision to choose the IASI measurements was made by taking into account their relatively high sensitivity in the boundary layer (George et al., 2009), as well as previous studies in which the IASI data were successfully employed for constraining CO emissions from different sources (Fortems-Cheiney et al., 2009; Krol et al., 2013; Konovalov et al., 2014). We considered the relatively high sensitivity of the IASI measurements in the lower troposphere as an important advantage, especially in the context of the given study involving a mesoscale CTM. Indeed, the upper troposphere CO content simulated with such a CTM is likely to be strongly affected by boundary conditions which are specified by using global CTM simulations and therefore are not dependent on CO emissions used in the regional CTM (see, e.g., a discussion in Konovalov et al., 2011). Exploring the potential of the alternative CO data products goes beyond the scope of the given study.

2.2 CTM simulations and initial processing of the model output data

In this study, the relationships between NO_x and CO emissions and, respectively, NO_2 and CO column amounts are simulated by the CHIMERE CTM. CHIMERE is a three-

dimensional Eulerian model designed to simulate air pollution on urban, regional, and continental scales; it allows to take into account the most important atmospheric processes (such as anthropogenic, biogenic, and fire emissions, gas-phase and heterogeneous chemistry, advection, turbulent diffusion, deep convection, dry and wet deposition) affecting the atmospheric fate of a number of reactive gaseous and aerosol species (see Menut et al., 2013, and references therein). The model was earlier successfully used in combination with satellite NO_2 and CO retrievals in several inverse modeling studies of NO_x and CO emissions (e.g., Konovalov et al., 2006, 2008, 2010, 2014; Berezin et al., 2013; Mijling and van der A, 2012; Ding et al., 2015).

In this study, the CHIMERE model was run with one of the standard domains (called the CONT5 domain) covering a western part of Europe (−13.75–25.25° E, 34.75–58.25° N) with the horizontal resolution of 0.5° × 0.5°. The simulations were performed with 12 non-equidistant layers in the vertical (up to the 200 hPa pressure level); the layers were specified in the hybrid sigma–pressure coordinates such that the distance between the layers increased with the altitude from ∼ 50 m near the surface to ∼ 2 km in the upper part of the modeled atmosphere. Gas-phase chemical processes were simulated with the simplified MELCHIOR2 chemical mechanism (Schmidt et al., 2001), and several heterogeneous reactions on the surfaces of aerosol particles were taken into account as described in Menut et al. (2013). Initial and boundary conditions for several key gaseous species responsible for the oxidation capacity of the lower atmosphere (e.g., CO, NO, NO_2, O_3, H_2O_2, HCHO) and aerosols were specified using monthly climatological data from LMDz-INCA global model (Folberth et al., 2006). A full list of these species is provided in the CHIMERE documentation available on the web site www.lmd.polytechnique.fr/chimere. An influx of other species, most of which are very reactive and short-lived (such as OH and HO_2), into a model domain is not specified in CHIMERE. Meteorological data were obtained from the WRF-ARW (v.3.6) model (Skamarock et al., 2008), which was run with a horizontal resolution of 50 km × 50 km and with 30 levels extending in the vertical up to the 50 hPa pressure level for a region covering the CHIMERE domain and was driven with the NCEP Reanalysis-2 data (National Centers for Environmental Prediction, 2000). The anthropogenic, biogenic, and fire emissions of major gaseous and aerosol species were taken into account in our simulations as described in the next section (Sect. 2.3). The model was run with different scenarios (specified below in Sect. 3.2) for the period from 22 December 2007 to 29 December 2008. The spin-up period included the first 10 days of any run, which therefore were withheld from the following analysis.

To enable consistency of our simulations with the satellite data employed in this study, the CHIMERE outputs were processed by taking into account measurement properties. All the simulated NO_2 and CO vertical profiles corresponding (in time and space) to any pixel that contained, respectively, the OMI and IASI measurements satisfying to the criteria specified in Sect. 2.1 were projected into the measurement vertical grids and transformed into tropospheric NO_2 columns and total CO columns, $C_m^{NO_2}$ and C_m^{CO}, by applying the respective averaging kernels, $\boldsymbol{A}^{NO_2}$ and $\boldsymbol{A}^{CO}$.

Specifically, the simulated NO_2 profiles were transformed as follows (Eskes and Boersma, 2003):

$$C_m^{NO_2} = \left(\boldsymbol{A}^{NO_2}\right)^T \boldsymbol{C}_{m(o)}^{NO_2}, \quad (1)$$

where $\boldsymbol{C}_{m(o)}^{NO_2}$ are the original model outputs (partial columns) interpolated to the pressure grid of the averaging kernels up to the tropopause pressure level (specified in the measurement database). Note that in relatively rare cases (constituting less than 20 % of the total number of valid observations available for the study region and period) where the tropopause pressure was smaller than the pressure at the top of the model grid (200 hPa), the lack of the simulated data at altitudes exceeding the height of the upper model layer could result in some underestimation of the modeled tropospheric columns, but such a minor inconsistency between the modeled and simulated NO_2 columns is not expected to result in underestimation of NO_x emissions in our analysis, owing to application of a debiasing technique described in Sect. 3.2 and validated in Sect. 3.5.

A slightly different procedure was used to process the modeled CO partial columns:

$$C_m^{CO} = (\boldsymbol{A}^{CO})^T \left(\boldsymbol{C}_{m(o)}^{CO} - \boldsymbol{C}_a^{CO}\right) + \boldsymbol{I}^T \boldsymbol{C}_a^{CO}, \quad (2)$$

where $\boldsymbol{C}_a^{CO}$ is the a priori CO vertical profile used in the retrieval procedure, and $\boldsymbol{I}$ is the identity vector. The missing components of $\boldsymbol{C}_{m(o)}^{CO}$ for altitudes above the upper layer of the CHIMERE CTM were taken to be equal to the respective values from $\boldsymbol{C}_a^{CO}$. Note that the transformation providing the total CO columns in accordance to Eq. (2) is a special case of the more general transformation procedure providing partial CO columns (see Fortems-Cheiney et al., 2009).

The model outputs transformed with different averaging kernels but corresponding to the same model grid cell and hour as the observations were averaged. The modeled profiles which had not been matched with the corresponding observational data were not used in our analysis. With the satellite data used in this study, each grid cell is provided with observed or modeled data for at most two different hours of each day. In addition to the selection criterion based on the DOFS values (see Sect. 2.1), in order to minimize the impact of model errors that are not associated with uncertainties in emission data on inverse modeling results, only those days and grid cells were taken into account when and where the modeled contribution of anthropogenic NO_x or CO emissions in the study region (specified in the next section) to $C_m^{NO_2}$ and C_m^{CO} was larger than one percent of the corresponding "background" values of the columns (here

"background" is defined according to a simulation made without anthropogenic emissions, i.e., with the biogenic and open biomass burning emissions specified in the next section, and with the transport model boundary conditions described above).

2.3 Emission inventory data

We used annual anthropogenic emission data for the year 2008 from several sources: the European Monitoring and Evaluation Programme (EMEP) regional emission inventory (EMEP/CEIP, 2014; Mareckova et al., 2014), the Emission Database for Global Atmospheric Research, version 4.2 (EDGAR v4.2) (EC-JRC/PBL, 2011), and the Carbon Dioxide Information Analysis Center (CDIAC) (Boden et al., 2011). The EMEP inventory data were used in our simulations described in Sect. 2.2, and the EDGAR v.4.2 data were used to relate the emission estimates for the proxy species with CO_2 emissions (see Sect. 3.3). The CDIAC data were involved in the analysis of uncertainties in our emission estimates (see Sect. 3.4) along with the EMEP and EDGAR v4.2 data.

The EMEP/CEIP inventory is based on emission data reported under the Convention on Long-range Transboundary Air Pollution by individual countries in Europe and in the Middle East, which are expected to use a unified approach (EMEP/EEA, 2013) applicable on the national level. In this study, we used the EMEP anthropogenic annual emission data distributed among 11 Selected Nomenclature for Air Pollutants (SNAP) sectors and provided for several pollutants, such as NO_x, CO, non-methane hydrocarbons (NMHC), SO_x, and particulate matter, on a grid with the resolution of $0.5^\circ \times 0.5^\circ$. Note that the EMEP inventory does not provide data for CO_2 emissions and that the emissions for the 11th sector (comprising biogenic sources and fires associated with human activities) were replaced in our simulations with data of dedicated inventories (as described in this section below).

The EDGAR v4.2 inventory is created by using the energy activity data provided by the International energy agency (IEA, 2010) and by following the methodology and fuel-specific emission factors based on the 2006 IPCC guidelines (IPCC, 2006). The IEA data were compiled following harmonized definitions of fuels and activities and applying the same methodologies across most countries (and some groups of countries outside of the study region). We used the EDGAR v4.2 data for the national totals of anthropogenic NO_x, CO, and CO_2 emissions distributed between several emission sectors (not necessarily coinciding with the SNAP sectors). Note that we used the EDGAR v4.2 FF CO_2 emission data excluding CO_2 emissions from biofuel burning (that is, the data used were calculated after "excluding short-cycle organic carbon"), while the corresponding CO and NO_x data included emissions from both fossil-fuel and biofuel burning.

The FF CO_2 emission data provided by CDIAC are based on the energy statistics that were compiled primarily from the annual energy questionnaire distributed by the United Nations Statistics Division and supplemented by official national statistical publications (UN, 2012). The quantity of fuel was converted into the quantity of CO_2 emissions by using the methodology based on Marland and Rotty (1984). The CDIAC database used in this study reports only national totals of FF CO_2 emissions without sectorial breakdowns and was used in this study for evaluation of uncertainties in our results.

Note that CO_2 emissions from cement production have been reported in CDIAC (as well as in EDGAR v4.2) separately from FF CO_2 emissions and were not considered in our study. Excluding this emission source from our estimates seems to be reasonable, taking into account that cement production, unlike FF burning, is not associated with considerable emissions of either NO_x or CO, and so satellite measurements of the corresponding proxy species cannot provide strong constraints on CO_2 emissions from cement production.

The anthropogenic emissions were aggregated into two categories. Splitting the total emissions among the two categories was deemed to reduce the generation of aggregation errors (Kaminski et al., 2001) in our top-down estimate of the total NO_x and CO emissions. To this end, we tried to ensure that, on the one hand, the emissions corresponding to the different categories had distinct spatial distributions (such as the emissions from power plants and from transport) and, on the other hand, that the amounts of annual emissions from each category were of the same order of magnitude. Specifically, the first category (EHI) included the emissions associated mostly with energy and heat production and heavy industries. The second category (TCO) comprised transport, chemical industry, and all other anthropogenic sources. In the EMEP inventory, the EHI category was defined by aggregating the sources corresponding to the first, second, and third sectors of SNAP (combustion in energy and transformation industries, nonindustrial combustion plants, and combustion in manufacturing industry, respectively). The sectors 1A1a-c (public electricity and heat production, other energy industries), 1A2 (manufacturing industries and construction), and 1A4 (fuel combustion in residential and other sectors) were allocated into the same category in the case of the EDGAR inventory. The TCO category aggregated all other anthropogenic sources considered in the EMEP or EDGAR v4.2 inventories. We expected that, apart from limiting the aggregation error, consideration of these two categories would allow us to get more specific information on emission sources. Note that splitting emission sources between the two categories specified above is, at large, rather arbitrary: in this study, we did not attempt analyzing the impact of the source categories definitions on the uncertainty of our emission estimates.

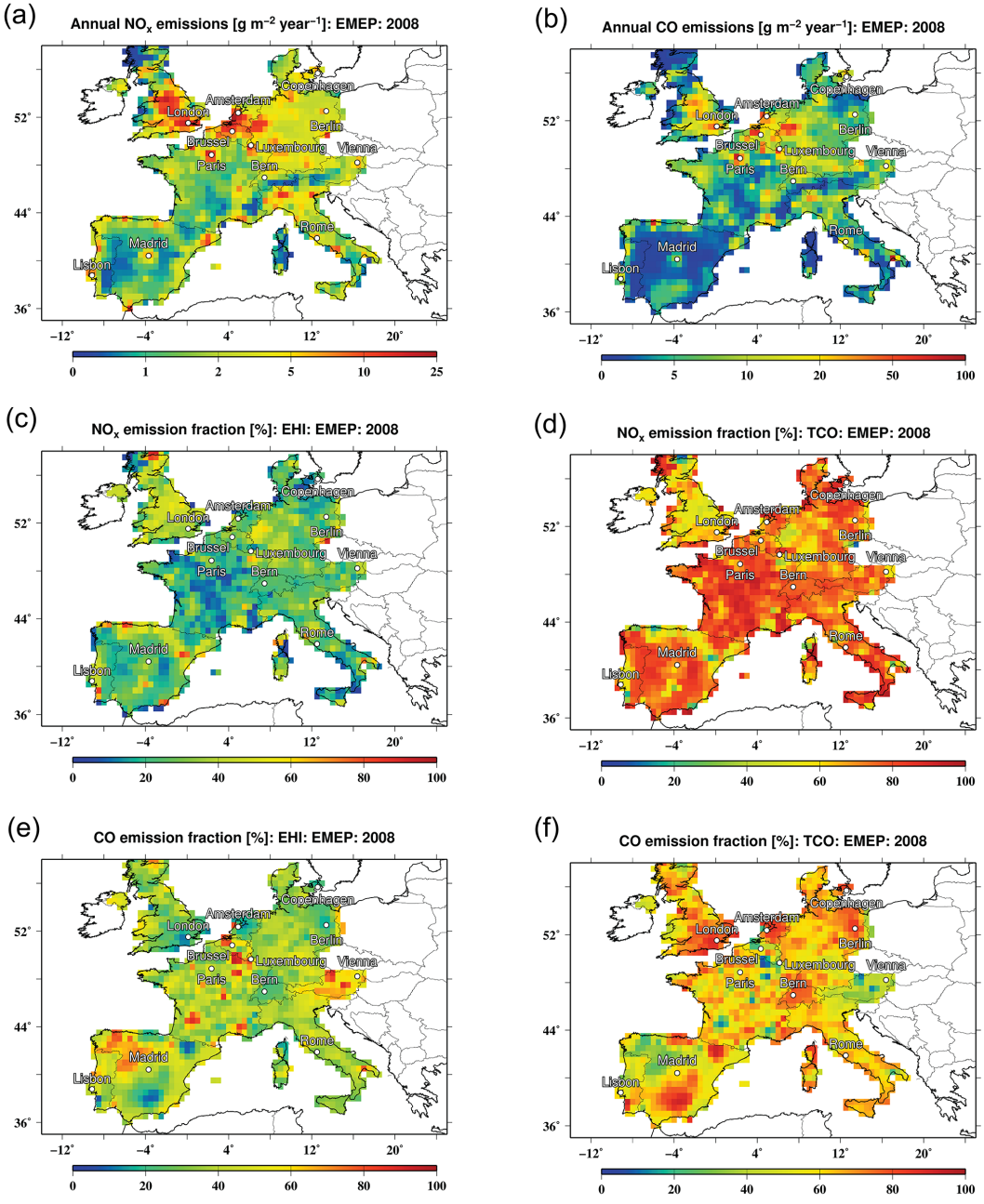

Figure 1. Spatial distributions of NO_x **(a)** and CO **(b)** total annual emissions ($g\,cm^{-2}\,yr^{-1}$) and the fractions (%) of the EHI **(c, e)** and TCO **(d, f)** emission source categories (see the definitions in Sect. 2.3) according to the EMEP inventory for 2008. The emission data are shown only for the study region comprising land territories of 12 European countries.

Figure 1 shows the CONT5 domain (employed in this study) of the CHIMERE CTM along with the spatial distributions of total annual anthropogenic NO_x and CO emissions from the selection of 12 western European countries considered in our analysis according to the EMEP inventory for 2008; it also shows the fractions of the two source categories introduced above. Note that emissions outside of the selected countries (including ship emissions) are not indicated (the corresponding territories are left blank), such emissions constitute minor parts of the total NO_x and CO emissions in the whole model domain shown in Fig. 1 (41 and 30 %, respectively, according to the EMEP inventory for 2008). The territory of the United Kingdom is not fully represented in the model domain; however, the emissions from the missing northern part of this country are rather negligible (~ 0.5 % of the total emissions in UK).

It is noteworthy that not only the total emissions (see Fig. 1a, b) but also the fractions of the different emission source categories (see Fig. 1c–f) exhibit considerable spatial variations. The spatial variability of the source category fractions indicates that, given sufficiently accurate observations, an appropriate inverse modeling procedure together with the dense spatial sampling of the atmosphere by satellites may have a potential to distinguish between emissions coming from the different sources. It can also be noted that the fractions of the same source categories of the NO_x and CO emissions considerably differ (cf. Fig. 1c–f). In particular, while the NO_x emissions mostly come from the TCO sources, the CO emissions are distributed between the TCO and EHI sources much more evenly. This observation indicates that the measurements of these two proxy species might provide complementary (to a certain extent) information on human activities associated with CO_2 emissions, even if atmospheric fates of the CO and NO_x emissions were identical.

The annual anthropogenic emission data were distributed at shorter timescales by applying monthly, daily, and hourly factors from the standard emission interface of the CHIMERE CTM (Menut et al., 2013); the factors were provided for specific pollutants, the SNAP sectors, and countries by IER, University of Stuttgart (GENEMIS, 1994). The seasonal variations specified in this way for the two categories of anthropogenic emissions are shown in Fig. 2. In addition, emissions were vertically distributed within 1 km by using the profiles (specific for each SNAP sector) provided in the emission interface of CHIMERE. Note that the vertical profiles did not explicitly account for aircraft emissions, which are also included in the EMEP inventory, but are likely to provide a very small contribution (less than 2 %) to anthropogenic NO_x and CO emission in Europe (Tarassón et al., 2004).

Along with the anthropogenic emissions, our model included biogenic emissions (in particular, NO_x emissions from soils and emissions of isoprene and some other hydrocarbons from vegetation) and emissions of gaseous species (NO_x, CO, and non-methane hydrocarbons) from open biomass burning (fires). Biogenic emissions were calculated for each grid cell, day, and hour within the CHIMERE model by using the European inventory of soil NO emissions (Stohl et al., 1996) and the emission factors and parameterizations from the MEGAN (Model of Emissions of Gases and Aerosols from Nature) model (Guenther et al., 2006). The fire emissions were specified using the daily data provided by the Global Fire Assimilation System, version 1.0 (GFAS v1.0) fire emission inventory (Kaiser et al., 2012). The fire emissions were distributed in the vertical uniformly up to the altitude of 1 km (similar to Konovalov et al., 2011). Note that according to the data of the GFAS v1.0 and EMEP emission inventories, the total emissions of both NO_x and CO from fires in the countries considered (mainly, in Portugal) in 2008 were rather small (~ 0.5 and ~ 5 % relative to the corresponding FF emission estimates given by the EMEP inventory).

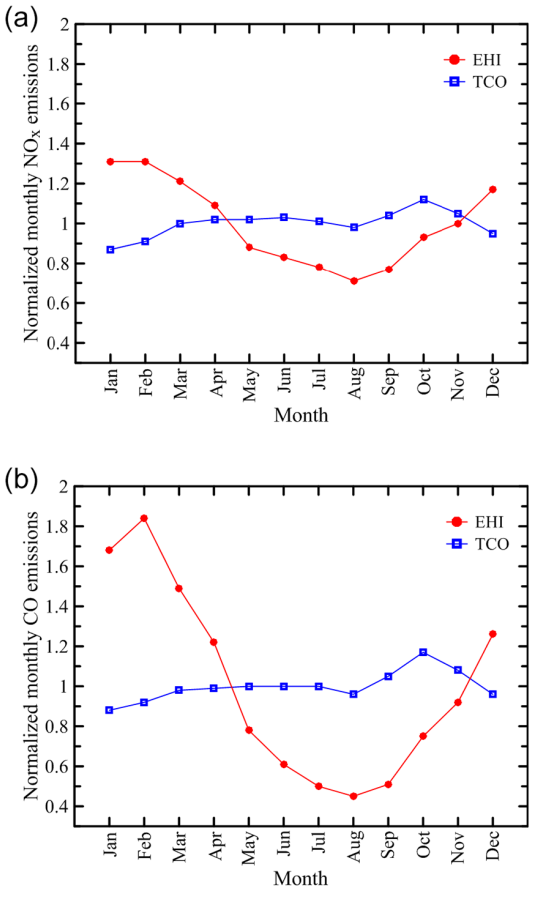

Figure 2. The seasonal variations of the spatially averaged (over the study region) NO_x **(a)** and CO **(b)** emissions for the EHI and TCO categories of sources. The variations were calculated as explained in Sect. 2.3. The values shown (unitless) are the monthly emissions normalized to the total annual emissions divided by 12.

2.4 Preliminary comparative analysis of the measurement and simulation data

In this section, we compare the measurement and simulated data and assess to what extent the variability of the NO_2 and CO columns over the study region is affected by direct anthropogenic emissions in the same region. Figure 3 shows time series of the daily values of NO_2 and CO columns averaged over the study region (see Fig. 1). The model was run both with and without anthropogenic emissions in the study region, and the model results are presented in Fig. 3 after compensating for a systematic difference with the measurements. The systematic difference (the bias) was evaluated as the average difference between the model data (obtained by running CHIMERE with full emissions) and the corresponding measurements. The averaging was carried out either directly for the whole annual period considered (see Fig. 3a, b)

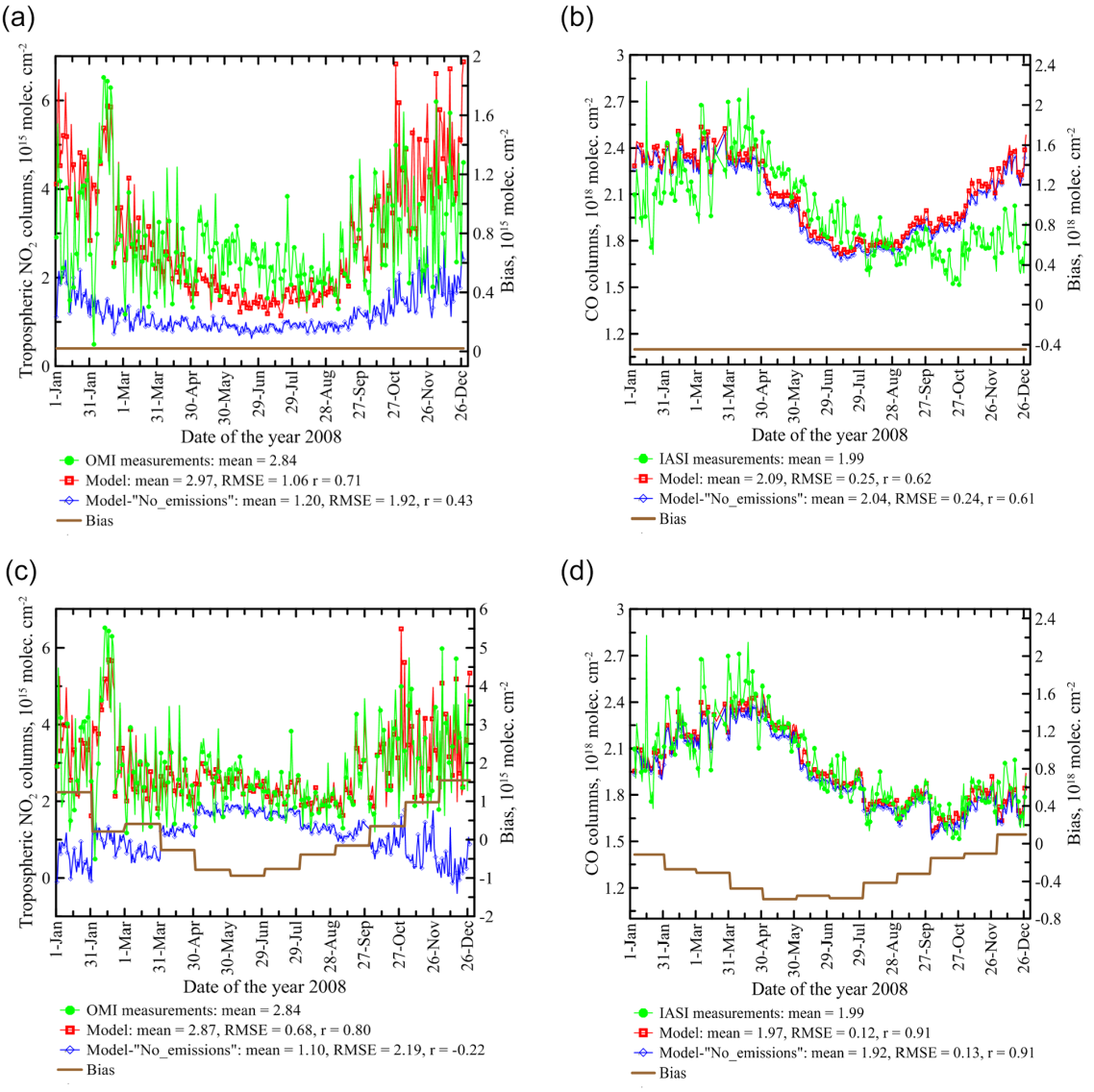

Figure 3. Time series of the spatially averaged NO_2 **(a, c)** and CO **(b, d)** columns retrieved from satellite measurements (see green curves) and simulated using the CHIMERE CTM both with and without anthropogenic emissions in the study region (see red and blue curves, respectively). The simulated data shown have been debiased: the differences (see brown curves) between either the annual **(a, b)** or monthly **(c, d)** averages of the simulation and measurement data were subtracted from the original simulation data.

or for each month independently (see Fig 3c, d). Note that the modeled NO_2 and CO columns shown in Fig. 3 were sampled consistently (both in time and space) with the respective available satellite data and processed using averaging kernels (see Sect. 2.2 and Eqs. 1 and 2); a very small difference between the CO columns calculated with and without anthropogenic emissions in the study region partly reflects the relatively low sensitivity of the CO retrievals in the boundary layer (compared to the upper troposphere).

It can be seen that both the NO_2 and CO measurements exhibit strong day-to-day variability. A part of the observed variability is captured by the model, but the amplitude of the variations is typically smaller in the simulations than in the measurements. Exact reasons for the stronger day-to-day variations in the measurements are not known: one possible reason is that the variations in the measurements may reflect random errors in the retrieval procedures (see Sect. 2.1), while another possible reason is that a part of the variations in the measurements may be due to factors which are not taken into account in our model (such as daily variability in the boundary conditions). Apart from the day-to-day variations, both the NO_2 and CO columns manifest slower variations. Such variations have a seasonal component in both the measured and simulated NO_2 columns, with larger values ob-

served in winter than in summer. A regular seasonal variability is visible also in the simulated CO data; however, similar variability in the corresponding measurement data appears to be offset by slower (probably interannual) variability, which is not reflected in the boundary conditions of CHIMERE. The differences between the measurements and simulations vary from month to month, thus indicating the importance of evaluating the biases on shorter than annual timescales; this observation is taken into account in our inversion procedure described in Sect. 3.2. It should be noted that the seasonal changes in the monthly biases may partly be due to errors in the seasonal cycles of the emissions specified in CHIMERE and in the global models that were used to obtain the a priori NO_2 and CO profiles for the respective retrieval procedures (see Boersma et al., 2011, and George et al., 2009, for details); such changes may also be indicative of some errors in the assumed seasonal variations of other parameters of the retrieval procedures, such as surface reflectance or atmospheric scattering by clouds and aerosol in the case of the NO_2 retrievals and surface temperature, local emissivity, vertical distributions of atmospheric temperature, and humidity in the case of the CO retrievals. Figure 3 also shows that while the anthropogenic emissions in the study region provide the predominant contribution to the NO_2 columns over the same region, the respective signal in the CO columns is very small.

Figure 4 presents the spatial distributions of the annually averaged NO_2 and CO columns derived from OMI and IASI measurements and simulated with the CHIMERE CTM. Note that only the data taken into account in our analysis are shown. NO_2 columns from both the measurements and simulations show very strong spatial variability correlating with the spatial distribution of NO_x emissions (cf. Figs. 4a, c and 1a); this observation is coherent with findings of earlier studies (e.g., Konovalov et al., 2006; Napelenok et al., 2008; Mijling et al., 2012) demonstrating that satellite retrievals of NO_2 columns combined with CTM outputs can provide useful information on the spatial distribution of NO_x emissions on a regional and even local (e.g., cities) scale. However, the simulations do not reproduce the spatial variability of NO_2 columns perfectly. In particular, the NO_2 column amounts over the hot spots located in the heavily industrialized Po Valley in Northern Italy, as well as over an industrialized region in the northwestern Germany and Madrid, are considerably smaller in the simulations than in the measurements; in contrast, the simulated NO_2 column amounts tend to be larger than the satellite retrievals over Great Britain. These differences may be due to uncertainties in the spatial distribution of NO_x emissions as well as to measurement and simulation errors.

Consistent with the results shown in Fig. 3, the signal from anthropogenic emissions appears to be rather weak and "smeared" in the spatial distribution of the CO columns. There are also big differences between the retrievals and simulations in some locations. Both the retrieved and simulated CO column amounts tend to be elevated over areas where the anthropogenic emissions are particularly large (such as those in Belgium, Germany, England, or the Po valley in Italy). However, Fig. 4f, showing the CO columns simulated without anthropogenic CO emissions in the study region and transformed using averaging kernels (see Eq. 2), bears evidence that an "anthropogenic signal" in the spatial variations of the measured CO columns may come mostly from the a priori CO columns employed in the retrieval procedure. Therefore, the preliminary analysis presented in this section indicates that the NO_2 measurements can potentially provide much stronger constraints for anthropogenic emissions on a regional scale compared to the CO measurements.

3 Method

3.1 Preliminary remarks

Our method is first described below for a rather general case (with arbitrary numbers of proxy species and emission source categories and for an arbitrary region); some settings specific for this study are either explained later or have been discussed in Sect. 2. The main steps of the method were briefly outlined in Introduction. The key step of the method – namely, the estimation of annual emissions of a proxy species from different categories of sources (emission sectors) in a region of interest – is described in Sect. 3.2. This step involves optimization of the emissions for a given sector by fitting simulations performed with a CTM to satellite observations of a corresponding species. An important element of the first step is the estimation and elimination of a possible systematic discrepancy between the simulations and observations which is not related to uncertainties in a priori emission data. Further steps leading to the estimation of the budgets of FF CO_2 emissions are described in Sect. 3.3. An important part of the method is dedicated to the estimation of the confidence intervals for all our emission estimates (see Sect. 3.4).

3.2 Optimization of emissions of proxy species

We estimate annual totals of anthropogenic emissions, E_c^s, from different categories of sources, c ($c \in [1, N_c]$, where N_c is the total number of categories), for a given proxy species, s, in a study region. To do that, we combine observations, $\boldsymbol{C}_o^s$, of the species atmospheric column amounts with respective modeled data, $\boldsymbol{C}_m^s$, by assuming (similar to, e.g., Berezin et al., 2013) that $\boldsymbol{C}_m^s$ depends on the emissions of a corresponding species linearly:

$$\boldsymbol{C}_m^s \cong \boldsymbol{C}_{mb}^s + \sum_c \mathbf{S}_c^s \boldsymbol{a}_c^s (E_c^s - \widetilde{E}_c^s), \quad (3)$$

where $\widetilde{E}_c^s$ are the available (a priori) bottom-up annual anthropogenic emission estimates for a species s and a source category c, $\boldsymbol{a}_c^s$ is the vector specifying allocation of the annual anthropogenic emissions to each cell of model's grid

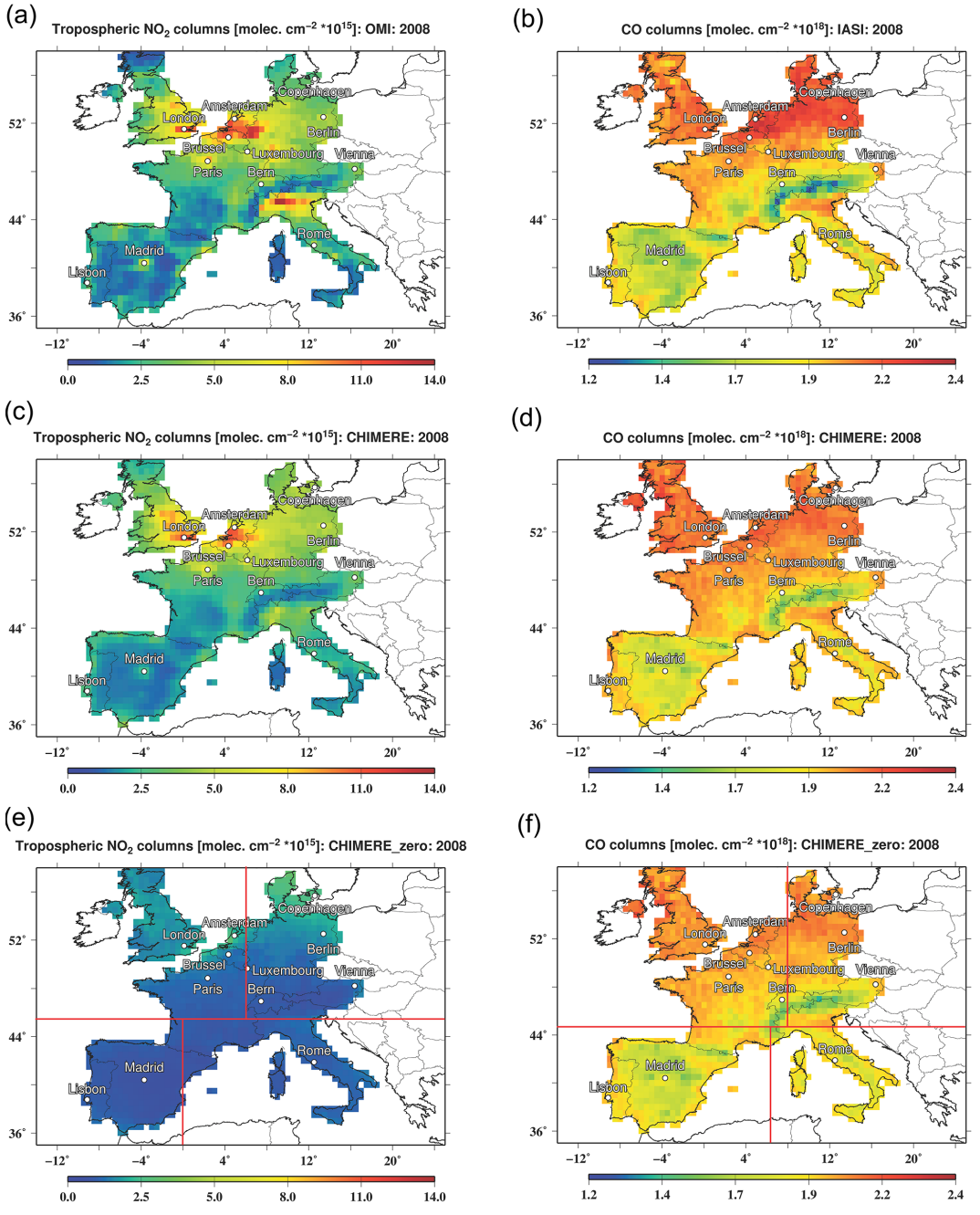

Figure 4. Spatial distributions of the annually averaged NO_2 **(a, c, e)** and CO **(b, d, f)** columns obtained from satellite observations **(a, b)** and model runs performed with **(c, d)** and without **(e, f)** anthropogenic emissions in the study region. Red lines **(e, f)** depict four subregions used in the uncertainty analysis described in Sect. 3.4; the subregions contain approximately the same amounts of daily data. Note that the simulation data have been debiased (in the same way as the data shown in Fig. 3a, b). Note also that the data which are not taken into account in our inverse modeling analysis are not shown.

and each day of the simulations, $\mathbf{S}_c^s$ is the Jacobean matrix containing sensitivities of the model outputs to the emissions, and $\boldsymbol{C}_{mb}^s$ are the species amounts calculated in a "base" model run using the bottom-up emission inventory data. Note that in this study, Eq. (3) was used specifically to express the modeled relationships between NO_2 measurements and NO_x emissions, as well as between CO measurements and CO emissions.

The annual emission estimates for individual source categories, E_c^s, constitute the control vector of our inverse problem, $\boldsymbol{E}^s$. The optimum estimate of $\boldsymbol{E}^s$ can be obtained by minimizing the sum of the squared differences between the

observations and simulations as follows:

$$\hat{\boldsymbol{E}}^{\mathrm{s}} = \mathrm{argmin}\left(\boldsymbol{C}^{\mathrm{s}}_{\mathrm{o}} - \boldsymbol{C}^{\mathrm{s}}_{\mathrm{m}} + \boldsymbol{\Delta}^{\mathrm{s}}\right)^{\mathrm{T}}\left(\boldsymbol{C}^{\mathrm{s}}_{\mathrm{o}} - \boldsymbol{C}^{\mathrm{s}}_{\mathrm{m}} + \boldsymbol{\Delta}^{\mathrm{s}}\right), \quad (4)$$

where $\hat{\boldsymbol{E}}^{\mathrm{s}}$ is the optimal estimate of the control vector, and $\boldsymbol{\Delta}^{\mathrm{s}}$ denotes the systematic discrepancies between the simulations and observations of a given proxy species s. Note that different components of the vectors $\boldsymbol{C}^{\mathrm{s}}_{\mathrm{o}}$, $\boldsymbol{C}^{\mathrm{s}}_{\mathrm{m}}$, and $\boldsymbol{C}^{\mathrm{s}}_{\mathrm{mb}}$ are assumed to represent available values of the respective columns amounts of the species s in different grid cells and/or different moments of time in the region and period considered.

The estimation given by Eq. (4) formally implies that the errors are homoscedastic, normally distributed, and uncorrelated in space and time; deviations of real data from these ideal assumptions can result in errors in $\hat{\boldsymbol{E}}^{\mathrm{s}}$, but we attempt to take such errors into account in respective confidence intervals for $\hat{\boldsymbol{E}}^{\mathrm{s}}$ (see Sect. 3.4). The systematic discrepancies $\boldsymbol{\Delta}^{\mathrm{s}}$, which are assumed to be independent of emission uncertainties and are estimated as explained below, can, in principle, be due to systematic errors both in the simulations and observations. For definiteness, $\boldsymbol{\Delta}^{\mathrm{s}}$ is assumed in this study to be due to biases in the simulations; the vector $\boldsymbol{\Delta}^{\mathrm{s}}$ is referred to below as simply "the bias". Formally, it can be defined as follows:

$$\boldsymbol{\Delta}^{\mathrm{s}} = \langle \boldsymbol{C}^{\mathrm{s}}_{\mathrm{m}} - \boldsymbol{C}^{\mathrm{s}}_{\mathrm{o}} \rangle, \quad (5)$$

where the brackets denote the averaging over the assumed statistical ensemble of probable values of $\boldsymbol{C}^{\mathrm{s}}_{\mathrm{m}}$ and $\boldsymbol{C}^{\mathrm{s}}_{\mathrm{o}}$ in a situation when the anthropogenic emissions in the study regions are known exactly.

Note that Eq. (4) does not include any formal a priori constraints on the magnitude of the optimal emission estimates (unlike many other inverse modeling studies) or any other regularization terms, and, accordingly, our procedure does not involve any explicit quantitative settings for the a priori error covariance matrices. In this way, we avoid possible uncertainties in optimal emission estimates that could be associated with such settings. Not using a priori constraints on the magnitude of the optimal emission estimates also enhances the value of the CO_2 emission estimates derived from completely independent measurements of different proxy species for cross-validation purposes, because otherwise the top-down estimates of emissions of the proxy species (and, accordingly, hybrid estimates of CO_2 emissions) could be more strongly dependent on the data of bottom-up inventories providing a priori estimates. Avoiding formal a priori constraints (or any other regularization) does not necessarily result in ill-conditioning of an inverse problem, as long as the dimension of the control vector does not exceed that of the measurement vector (Enting, 2002), and it is definitely so in our case. Although satisfying this criterion alone cannot guarantee that the problem is well conditioned, the numerical experiments presented below in Sect. 3.5 indicate that errors in our emission estimates due to probable errors in input data remain limited and thus the problem considered in this study is not ill conditioned. The dimension of the control vector (one or two) is much smaller, in our case, than that of the measurement vector (including tens of thousands of observations) because we do not attempt improving the allocation of the emissions in space and time: the vectors $\boldsymbol{a}^{\mathrm{s}}_{\mathrm{c}}$ are assumed to be known (in practice, $\boldsymbol{a}^{\mathrm{s}}_{\mathrm{c}}$ are provided implicitly by an emission interface in a CTM). Similar assumptions are not unusual in inverse modeling studies involving CTMs (e.g., Pétron et al., 2004; Müller and Stavrakou, 2005; Huneeus et al., 2012), when the emissions are corrected for big regions rather than for each model grid cell individually: indeed, optimization of emissions of chemically reactive species (like NO_x) is, in a general case, a time-consuming task, even when an adjoint code is available. A drawback of fixing the spatial distribution of the emissions in inversion is a probable aggregation error (Kaminski et al., 2001). Similarly, errors in our total annual emission estimates can also result from fixing the temporal distribution of the emissions. For example, if the assumed seasonal cycle of the emissions overestimates them in summer and underestimates in winter, then, taking into account that more satellite observations are available in summer than in winter (because of seasonal differences in the atmospheric conditions), our annual estimates can be biased negatively. We attempted to take into account possible errors in our estimates due to errors in spatial and temporal allocation of the emissions in the uncertainty analysis (see Sect. 3.4).

We assess the bias for a given data point i as the average difference between the simulated and observed columns of a species s for the month m in which the data point i lies:

$$\Delta^{\mathrm{s}}_i \cong \left[\sum\nolimits_j \theta^{\mathrm{s}}_j(m)\right]^{-1} \sum\nolimits_j \left[\theta^{\mathrm{s}}_j(m)\left(C^{\mathrm{s}}_{\mathrm{m}j} - C^{\mathrm{s}}_{\mathrm{o}j}\right)\right], \quad (6)$$

$$\in \begin{cases} \theta^{\mathrm{s}}_j = 1, \ j \in \Omega_{\mathrm{m}} \\ \theta^{\mathrm{s}}_j = 0, \ j \notin \Omega_{\mathrm{m}} \end{cases},$$

where Ω_{m} denotes the subset of the available data for a given month m, and $i \in \Omega_{\mathrm{m}}$ is the index of a component (a point in time and space) of the vector $\boldsymbol{\Delta}^{\mathrm{s}}$. It should be noted that values of $\boldsymbol{C}^{\mathrm{s}}_{\mathrm{m}}$ in Eq. (6), like those in Eq. (4), depend on the control vector, $\boldsymbol{E}^{\mathrm{s}}$. When combined with Eqs. (3) and (6), Eq. (4) specifies a linear optimization problem that can be easily resolved numerically. Effectively, information about optimal values of the emission vector is obtained from spatial and temporal variations of the observations and simulations within each month.

Equation (6) provides a simple approximation for Eq. (5) by implying that the systematic differences between different pairs of simulations and observations corresponding to a given month are about the same; that is, we assume that the bias is uniform in space and time during a given month. In reality, however, systematic errors of satellite retrievals and model results can be different for different grid cells and days. Therefore, this approximation (which reflects the lack of any a priori information about the bias) may introduce

some extra errors in our emission estimates which would not appear if the structure of the bias were known exactly. Although we cannot avoid such errors, we try, at least, to take them into account in the confidence intervals for our estimates. Note that as long as there is only one realization of $\boldsymbol{C}_{\mathrm{m}}^{\mathrm{s}}$ and $\boldsymbol{C}_{\mathrm{o}}^{\mathrm{s}}$ for the region and period considered, an unambiguous separation between their random uncertainties and systematic errors is hardly feasible anyway.

Summing up the optimal emission estimates for the different source categories provides the estimate of total emissions, $\hat{E}_{\mathrm{sum}}^{\mathrm{s}}$, of the species s in the study region. Alternatively, the estimate of the total emissions can be obtained by applying the estimation procedure described above to the special case where all emission sources are aggregated together and $N_{\mathrm{c}} = 1$. The corresponding optimal emission estimates are denoted below as $\hat{E}_{\mathrm{tot}}^{\mathrm{s}}$. Considering the difference between $\hat{E}_{\mathrm{sum}}^{\mathrm{s}}$and $\hat{E}_{\mathrm{tot}}^{\mathrm{s}}$ provides a useful test for self-consistency of the inversion procedure: the difference should not exceed the combined confidence intervals (that are expected to include an aggregation error among other uncertainties) for $\hat{E}_{\mathrm{sum}}^{\mathrm{s}}$ and $\hat{E}_{\mathrm{tot}}^{\mathrm{s}}$.

The estimation method described above requires the knowledge of the product of the Jacobean matrix, $\mathbf{S}_{\mathrm{c}}^{\mathrm{s}}$, and of the vector $\boldsymbol{a}_{\mathrm{c}}^{\mathrm{s}}$ (see Eq. 3), while the knowledge of the Jacobean matrix itself is not needed. In this study, this product was evaluated as the difference between the results of a model base run performed with the standard emission settings as described in Sect. 2.3 and the results of the special runs (EHI or TCO) performed after decreasing the annual EMEP emission values for the respective (EHI or TCO) source categories by 10 %. The product of $\mathbf{S}_{\mathrm{c}}^{\mathrm{s}}$ and $\boldsymbol{a}_{\mathrm{c}}^{\mathrm{s}}$ in the case where all emission sources were aggregated together (that is, with $N_{\mathrm{c}} = 1$) was evaluated as the sum of the products of $\mathbf{S}_{\mathrm{c}}^{\mathrm{s}}$ and $\boldsymbol{a}_{\mathrm{c}}^{\mathrm{s}}$ for the two individual (EHI and TCO) emission categories.

Note that we analyzed only the measurements over land in the study region, and so the measurements outside of the study region (e.g., over ocean) were not used. Such a limitation affected the amount of data used in the analysis, but we do not see any reason to expect that it could result in any biases in our emission estimates, which would not be covered by their uncertainty intervals (evaluated as explained in Sect. 3.4). Likewise, we do not expect that any biases in our emission estimates can be caused by NO_x and CO emissions outside of the study region. Indeed, on the scales considered, it seems reasonable to regard temporal and spatial variations of NO_2 and CO originating from any sources (including ship emissions) outside of the study region as model errors on top of the modeled variations of NO_2 and CO originating from inside of the study region. Accordingly, we do not distinguish such variations from other errors and treat their systematic and random parts as explained in this section (see Eq. 6) and in Sect. 3.4, respectively.

3.3 Estimation of FF CO_2 emissions

Following Berezin et al. (2013), we introduce the conversion factors, $F_{\mathrm{c}}^{\mathrm{s}}$, describing the relationships between the annual emissions for a given proxy species s and the CO_2 emissions:

$$F_{\mathrm{c}}^{\mathrm{s}} = \frac{\widetilde{E}_{\mathrm{c}}^{\mathrm{CO_2}}}{\widetilde{E}_{\mathrm{c}}^{\mathrm{s}}}, \tag{7}$$

where $\widetilde{E}_{\mathrm{c}}^{\mathrm{CO_2}}$ and $\widetilde{E}_{\mathrm{c}}^{\mathrm{s}}$ are the annual estimates of anthropogenic CO_2 emissions and of anthropogenic emissions for a species s for a given emission source category (sector) c. Here (as above), the tildes indicate that the emission estimates are obtained from a bottom-up emission inventory (as opposed to the optimal emission estimates, $\hat{E}_{\mathrm{c}}^{\mathrm{s}}$, inferred from the measurements according to Eq. (4) by using the modeled relationships between the column amounts of a given proxy species and corresponding emissions).

Application of the conversion factors to the corresponding optimal emission estimates allows us to obtain the hybrid CO_2 emission estimates, $\hat{E}_{\mathrm{sc}}^{\mathrm{CO_2}}$, that are partly constrained by the measurements but also depend on data of the emission inventory:

$$\hat{E}_{\mathrm{sc}}^{\mathrm{CO_2}} = F_{\mathrm{c}}^{\mathrm{s}} \hat{E}_{\mathrm{c}}^{\mathrm{s}}. \tag{8}$$

Similarly, we can estimate the total CO_2 emissions:

$$\hat{E}_{\mathrm{s,\,sum}}^{\mathrm{CO_2}} = \sum_{\mathrm{c}} F_{\mathrm{c}}^{\mathrm{s}} \hat{E}_{\mathrm{c}}^{\mathrm{s}}. \tag{9}$$

The alternative total CO_2 emission estimate, $\hat{E}_{\mathrm{c,\,tot}}^{\mathrm{CO_2}}$, can be inferred directly from an estimate of the total emissions for a proxy species:

$$\hat{E}_{\mathrm{s,\,tot}}^{\mathrm{CO_2}} = F_{\mathrm{tot}}^{\mathrm{s}} \hat{E}_{\mathrm{tot}}^{\mathrm{s}}, \tag{10}$$

where $F_{\mathrm{tot}}^{\mathrm{s}}$ is the conversion factor evaluated similar to Eq. (7) but by using total annual emission estimates based on emission inventory data, and $\hat{E}_{\mathrm{tot}}^{\mathrm{s}}$ are the corresponding estimates inferred from satellite measurements. Note that the conversion factors that were used to obtain our hybrid FF CO_2 emission estimates reported below in Sect. 4.2 were calculated with the EDGAR v4.2 emission inventory data.

The hybrid CO_2 emission estimates derived from measurements of different species can be used for the cross-validation purposes (specifically, the different estimates are expected to agree within the range of their confidence intervals if all uncertainties including aggregation errors are adequately accounted for in the inversion procedure). They can also be combined by taking into account the uncertainty of the individual estimates. Specifically, given N_{s} individual emission estimates, $\hat{E}_{\mathrm{sc}}^{\mathrm{CO_2}}$, the combined (maximum likelihood) estimate of the CO_2 emissions, $E_{\mathrm{comb,\,c}}^{\mathrm{CO_2}}$, and its uncertainty

range can be expressed as follows:

$$\hat{E}^{CO_2}_{comb,c} = \left(\sum_{s=1}^{Ns}\left(\sigma^{CO_2}_{sc}\right)^{-2}\right)^{-1}\sum_{s=1}^{Ns}\hat{E}^{CO_2}_{sc}\left(\sigma^{CO_2}_{sc}\right)^{-2};$$
$$\sigma^{CO_2}_{comb,c} = \left(\sum_{s=1}^{Ns}\left(\sigma^{CO_2}_{sc}\right)^{-2}\right)^{-1/2}, \quad (11)$$

where $\sigma^{CO_2}_{sc}$ are the uncertainties (the standard deviations) of $\hat{E}^{CO_2}_{sc}$.

A combined estimate for the total CO_2 emissions, $\hat{E}^{CO_2}_{comb,tot}$, can be obtained in a similar way by using values of $\hat{E}^{CO_2}_{s,tot}$. An alternative combined estimate for the total emissions, $\hat{E}^{CO_2}_{comb,sum}$, can be obtained by summing up values of $\hat{E}^{CO_2}_{comb,c}$ for different source categories c. The standard deviations $\sigma^{CO_2}_{sc}$ can be evaluated as described in the next section (Sect. 3.4). Importantly, according to Eq. (11), the probable uncertainty of the combined estimate $\hat{E}^{CO_2}_{comb,c}$ is smaller than the uncertainty of any of the individual estimates. It should be noted, however, that Eq. (11) provides the maximum likelihood estimate only if the "input" emission estimates derived from measurements of individual proxy species are statistically independent from each other; otherwise it would be necessary to take into account their error covariances. Applicability of Eq. (11) to the situation addressed in this study is discussed in Sect. 4.2.

3.4 Uncertainties in the emission estimates

Evaluation of credible confidence intervals for our optimal emission estimates by using a typical error propagation technique requires proper knowledge of the statistical characteristics of model and measurement errors. However, in case of simulations and satellite measurements of minor atmospheric species, such knowledge is usually lacking due to complexity and multiplicity of factors that may lead to retrieval and model errors. Taking such considerations into account, instead of using the error propagation technique, we follow the so-called subsampling approach (Politis et al., 1999). Subsampling suggests estimating the confidence interval of a sample statistic (e.g., the variance) by considering variability of that statistic among subsamples drawn from the original sample without replacement.

To adopt the subsampling approach in this study, the original set (sample) of input data for a given proxy species s is divided into n_d subsets (subsamples). From each subset, a "partial" independent emission estimate, $\hat{E}^s_{c,i}$ ($i \in [1, n_d]$), is inferred. The partial estimates can be used to evaluate the standard error, σ^s_c, of $\hat{E}^s_c$ (that is, the standard error of the sample estimate) as follows:

$$\sigma^s_c \cong \sqrt{\frac{1}{n_{d(n_d-1)}}\sum_{i=1}^{nd}\left(\hat{E}^s_{c,i} - \hat{E}^s_{c(\bullet)}\right)^2}, \quad (12)$$

where $(\bullet)$ denotes the mean over all the partial estimates. Importantly, the estimation given by Eq. (12) requires the partial estimates to be statistically independent. If this condition is satisfied, the partial estimates, $\hat{E}^s_{c,i}$, that are involved in Eq. (12) can be regarded as independent observations of the same characteristic: deviations between $\hat{E}^s_{c,i}$ and $\hat{E}^s_{c(\bullet)}$ can only be due to errors in the simulated and measured data. In this sense, Eq. (12) essentially evaluates the standard deviation of the mean of individual observations (individual top-down emission estimates in our case) affected by random errors. Note that a simple and robust estimation technique involving Eq. (12) is basically the same as one of the oldest and popular techniques within the subsampling approach, known as replicated sampling (Deming, 1960; Lee and Forthofer, 2006). The standard errors in our estimates, $\hat{E}^s_{sum}$ and $\hat{E}^s_{tot}$, for the total emissions of proxy species can be evaluated in the same way (that is, by substituting $\hat{E}^s_{sum,i}$ and $\hat{E}^s_{sum(\bullet)}$ or $\hat{E}^s_{tot,i}$ and $\hat{E}^s_{tot(\bullet)}$ into Eq. (12) instead of $\hat{E}^s_{c,i}$ and $\hat{E}^s_{c(\bullet)}$).

The statistical independence of the partial estimates could not be ensured in our case if different subsets were selected in a quite arbitrary way. The reason is that the model and observation errors tend to covariate both in space and time (as confirmed by our analysis discussed below in Sect. 3.5). Thus, on the one hand, the data included in different subsets should be sufficiently separated in time and/or space to avoid co-variation of errors of different partial estimates. On the other hand, the number of the subsets should not be too small to ensure that the standard error estimate is sufficiently reliable (note that statistical inference defined by Eq. (12) is based on $n_d - 1$ degrees of freedom). It was also necessary to take into account that the error structure in temporal and spatial domains can be different.

In view of these considerations, we opted to divide the original dataset into four subsets in the temporal domain and four subsets in the spatial domain. Each of the subsets in the temporal domain included data for only one season but for the full spatial domain. The gridded data subsets for winter, spring, summer, and autumn months included 3.9×10^4, 4.1×10^4, 5.4×10^4, and 4.1×10^4 values in the case of NO_2 measurements and 2.6×10^3, 1.4×10^4, 2.5×10^4, and 1.2×10^4 values in the case of CO measurements. The spatial subsets were defined as shown in Fig. 4e, f and each included about 4.3×10^4 and 1.3×10^4 values for the whole year in the cases of NO_2 and CO measurements, respectively. The standard error was estimated in accordance to Eq. (12) independently for both "temporal" and "spatial" subsets (that is, n_d was equal 4 in the both cases), and the maximum of the two estimates of σ^s_c was selected as the final estimate of the standard error. Note that such a division allowed us to retain most of the actual error covariances within a given subsample, as the areas and time periods covered by each subset were significantly larger than expected error covariance scales (see Sect. 3.5 for further details). In contrast, selection of the maximum of the two different σ^s_c estimates may re-

sult in overestimation of the confidence intervals that can be robustly evaluated by applying t values (from the Student's distribution with three degrees of freedom in our case) to the standard error estimate.

We expect that apart from random errors in the input data, the error estimate obtained as described above also includes (at least to some extent) the aggregation error (Kaminski et al., 2001). In this study, that kind of error may be due to aggregation of similar sources in all the countries considered into a single component of the control vector. As contributions of various sources to the CO and (especially) NO_2 columns in the different countries are different, the aggregation error is likely to be manifested as deviations between the different partial estimates. For example, if, in a hypothetical situation, an emission estimate inferred from the full dataset were mostly affected by strong emission sources from only one country, a partial estimate obtained after leaving the measurements over that country out would likely be much less affected by the same sources, at least in the case of emission estimates of such a short-lived species as NO_x.

The confidence intervals estimated using Eq. (12) are also likely to account for most of estimation errors associated with uncertainties in the diurnal and weekly variations of anthropogenic emissions, as well as with uncertainties due to shortcomings in the model representation of chemical processes (including effects of subgrid-scale chemical interactions). Indeed, it seems reasonable to expect that different errors of the emission temporal cycles for different emission sectors, countries, and seasons can be manifested as quasi-random deviations between the simulations and measurements in different grid cells and days. Uncertainties in the diurnal variations of emissions are likely to be manifested additionally in the differences between the hybrid CO_2 emissions estimates inferred separately from the CO and NO_2 measurements, as those measurements are taken in different times of a day (see Sect. 2.1). Uncertainties in simulations of chemical processes and subgrid-scale chemical interactions are likely to have a different impact on the modeled NO_2 or CO columns in different types of environments (e.g., rural or urban) and in different seasons; therefore, the respective model errors are likely to differ in different grid cells (and days of an year) and to have a different impact on the NO_x or CO emission estimates for different subregions and seasons. Accordingly, it indeed seems reasonable to assume that such errors are mostly taken into account in the emission estimate uncertainties evaluated with Eq. (12). In addition, as the NO_2 and CO behaviors are governed by essentially different chemical processes, uncertainties due to a "chemical" part of model errors are likely to contribute to differences between the CO_2 emission estimates based on the NO_2 and CO measurements.

Note that it is nonetheless not quite infeasible that some model errors associated with the representation of chemical interactions can result in similar (positive or negative) biases across the NO_x or CO emission estimates inferred from the different data subsets. For example, systematic underestimations of the NO_x emissions may be due to persistent positive biases in the ozone formation rate and in boundary conditions for tropospheric ozone concentration (as ozone concentration accounts for partitioning of NO_x between NO and NO_2) as well as due to other numerous factors (such as underestimation of the hydrocarbon emissions or of the ozone photolysis rate) that may result in underestimation of concentration of hydroxyl radical providing a major sink for NO_x and determining its atmospheric lifetime (Seinfeld and Pandis, 2006). Depending on atmospheric conditions, effects of different model errors on the emission estimates may or may not compensate each other. Even though different model errors are likely to combine and affect the emission estimates in different ways in the different subregions and seasons, we cannot completely ensure that the confidence intervals for our CO and (especially) NO_x emission estimates actually account for all possible model errors. More accurate evaluation of effects of possible errors in the model representation of chemical processes on NO_x and CO emission estimates that can be derived from satellite measurements by using our inverse modeling method requires further research (involving, e.g., multi-model inversions) that goes beyond the scope of this study.

Uncertainties in the seasonal cycles of anthropogenic emissions are likely to be manifested (in the absence of any other model and measurement errors) as the differences between the annual emission estimates obtained with the four data subsets including data for the different seasons. Therefore, we expect that such uncertainties are also addressed in the confidence intervals evaluated as explained above. However, compared to the diurnal and weekly variations, uncertainties in the seasonal variations of emissions more probably result in common systematic biases of NO_x and CO emission estimates. To get an idea about the magnitude of such biases, we compared the emission estimates for the two cases involving simulations with different seasonal cycles. The first case (referred to below as the "cycle" case) corresponds to the standard seasonal cycles assumed in our model (see Fig. 2). The second ("flat") case corresponds to simulations performed with constant emissions in any month of a year (yet with the same diurnal and weekly emission temporal profiles as in the cycle case). Note that the differences between the emissions estimates obtained for these two cases are likely to strongly exceed the respective uncertainty (because the flat case is evidently unrealistic).

It should be noted that the qualitative considerations discussed above are by no means intended to strictly prove that the estimations based on Eq. (12) actually account for all possible errors. Nonetheless, taking the above arguments into account and given the fact that both the origins and the statistical characteristics of errors in the measurement, simulation, and inventory data involved in our analysis are very poorly known, we believe that the simple and robust subsampling technique described above provides sufficiently reliable and

robust uncertainty estimates and has no serious alternative in the situation considered. Some further arguments supporting reliability of this technique are discussed in Sect. 3.5.

To obtain the confidence intervals for our CO_2 emission estimates, we need to combine the uncertainty of our estimates of emissions of proxy species with the uncertainty of the corresponding conversion factors. Ideally, the uncertainty of the conversion factors for source categories that group different sectors (like EHI and TCO) could be obtained, e.g., by varying parameters of a bottom-up inventory (Wang et al., 2013) and provided along with emission data. However, in our knowledge, such information has unfortunately not yet been made available within any inventory except those by Wang et al. (2013) for China. As an alternative approach, we suggest that the uncertainty of the conversion factors can be roughly estimated by comparing their values based on data of different emission inventories. Ideally, it would be best to consider an ensemble of several independent inventories providing the data on emissions of all the species (NO_x, CO, and CO_2) involved in our analysis. However, in this study, in view of the limited practical availability of the necessary data, we realized only a highly simplified version of such an approach. Specifically, along with the conversion factors based on the EDGAR v4.2 emission inventory (those values were used to obtain our "main" CO_2 emission estimates as described in Sect. 3.3 and are denoted in this section simply as F_c^s), we considered "alternative" conversion factor values based on the data of other inventories, such as EMEP and CDIAC. The alternative conversion factor values are denoted below as $F_c^{s'}$. Specifically, we used the EMEP inventory data for NO_x and CO emissions and the CDIAC data for FF CO_2 emissions (see Sect. 2.3). Taking into account considerable differences in the data sources and methodologies used across the three inventories (see Sect. 2.3 and the corresponding references for details), we assume that the main and alternative conversion factor estimates are sufficiently independent. As the CDIAC emission data had not been originally distributed among individual emission sectors, the fractions of the two categories of the CO_2 sources were taken to be the same as in the EDGAR v.4.2 inventory. However, only the original CDIAC and EMEP data were used to estimate the conversion factors applied to the total emissions ($F_{tot}^{s'}$).

Using again the subsampling technique, we roughly estimated the standard error for the conversion factors, σ_{sc}^F, as follows:

$$\sigma_{sc}{}^F = \sqrt{\frac{1}{(N_k-1)N_k}\sum_{k=1}^{N}{}_k \left(F_{c,k}^s - F_{c,k}^{s'} - F_{c(\bullet)}^s + F_{c(\bullet)}^{s'}\right)^2 + \left(F_c^s - F_c^{s'}\right)^2}, \quad (13)$$

where $F_{c,k}^s$ and $F_{c,k}^s$ are the conversion factors evaluated individually for each of the 12 countries considered, c is the country index, N_k is the total number of the countries considered ($N_k = 12$ in this study), and $(\bullet)$ denotes the means over the countries. The country scale is used in Eq. (13), because the CDIAC data had not been provided on a spatial grid, and thus we could not consider the same spatial subsamples as those with the data for NO_2 and CO columns. The estimations given by Eqs. (12) and (13) are based on the same idea, except that unlike Eq. (12), Eq. (13) does not involve the assumption that the error of a "sample" estimate is completely random in origin; rather, it takes into account that the error may contain both random and systematic components. The latter is evaluated in Eq. (13) as the difference between the estimates F_c^s and $F_c^{s'}$ representing the full study region. Actually, that difference may include a part of the random error, so Eq. (13) is likely to overestimate σ_{cs}^F. Further overestimation may be due to the fact that the differences in Eq. (13) comprise cumulative errors in the both conversion factor estimates: if the errors were distributed equally between the main and alternative estimates, a proper value of σ_{cs}^F would be at least the factor of $2^{1/2}$ smaller than the one given by Eq. (13). In contrast, using the same (EDGAR v.4.2) data to evaluate both $F_{c,k}^s$ and $F_{c,k}^{s'}$ may compensate such an enhancement or even entail a tendency for underestimation in σ_{sc}^F (except for the case where the conversion factors and their uncertainties are estimated directly for total emissions, that is, without sectorial breakdowns). Nonetheless, on the whole, taking the above qualitative considerations into account, we expect that values of σ_{sc}^F calculated as described above are more likely to be overestimated than underestimated, thus being conservative in our approach to provide optimal CO_2 emission estimates.

Values of the conversion factors, F_{tot}^s and $F_{tot}^{s'}$, calculated using different inventories for each country considered are shown in Fig. 5. The differences between the different estimates of the conversion factors are, in general, considerable and vary across different countries in the study region. Specifically, the differences for the NO_x-to-CO_2 emission and CO-to-CO_2 conversion factors range from 1.4 to 24.9 % and from 3.8 to 52.6 % (relative the values based on the EDGAR v.4.2 data), respectively. The differences are smallest for Austria and Germany.

The standard error, $\sigma_{sc}^{CO_2}$, representing the uncertainty in our hybrid estimates of anthropogenic CO_2 emissions was estimated by assuming that uncertainties in the estimates of a proxy species emissions and in the estimates of the conversion factors are independent:

$$\sigma_{sc}^{CO_2} = \hat{E}_{sc}^{CO_2}\sqrt{\left(\frac{\sigma_c^s}{\hat{E}_c^s}\right)^2 + \left(\frac{\sigma_{sc}^F}{F_c^s}\right)^2}. \quad (14)$$

The standard error, $\sigma_{s,tot}^{CO_2}$, for a corresponding total CO_2 emission estimate, $\hat{E}_{s,tot}^{CO_2}$ (see Eq. 10), was evaluated in the same way. Taking into account that the uncertainties in the top-down estimates of emissions of proxy species for different source categories are likely not independent, the standard error, $\sigma_{s,sum}^{CO_2}$, of $\hat{E}_{s,sum}^{CO_2}$ (see Eq. 9) was given by a similar but

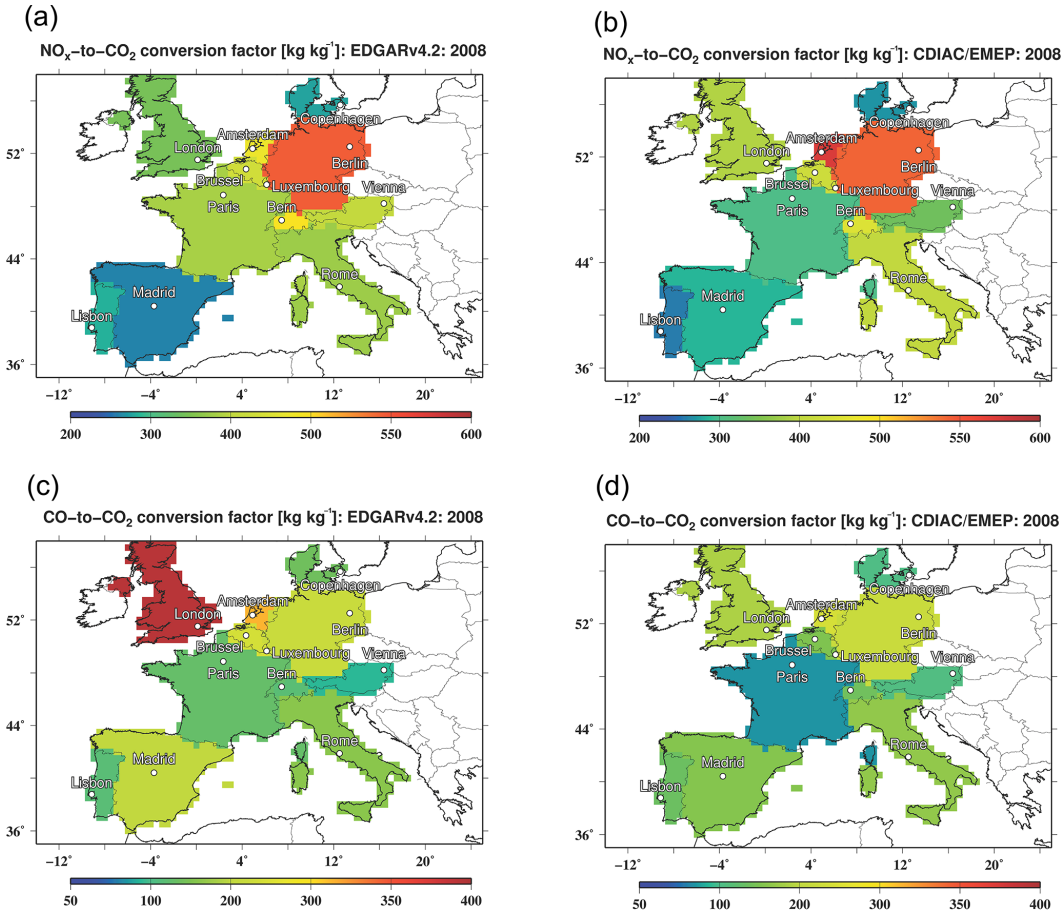

Figure 5. NO_x-to-CO_2 **(a, b)** and CO-to-CO_2 **(c, d)** emission conversion factors obtained using NO_x, CO, and CO_2 emission estimates from the EDGAR v4.2 emission inventory **(a, c)** and from the CDIAC and EMEP emission inventories **(b, d)** for the emission totals.

slightly more complicated equation:

$$\sigma^{CO_2}_{s,\,sum} = \sqrt{\sum_c \left(\hat{E}^s_c \sigma^F_{sc}\right)^2 + \left(\sigma^{CO_2|F}_{s,\,sum}\right)^2}, \quad (15)$$

where $\sigma^{CO_2|F}_{s,\,sum}$ represents the standard error of $\hat{E}^{CO_2}_{s,\,sum}$ under the condition that the conversion factors are known exactly (that is, the errors included in $\sigma^{CO_2|F}_{s,\,sum}$ are associated with only uncertainties of our top-down emission estimates for the proxy species); $\sigma^{CO_2|F}_{s,\,sum}$ was evaluated by using the same subsampling technique as described above for the case of estimation of uncertainties in $\hat{E}^s_c$. The standard errors given by Eqs. (14) or (15) allowed us to combine the estimates based on the measurement of NO_2 and CO columns by using Eq. (11).

3.5 Observation system simulation experiments (OSSEs; tests with synthetic data)

In this section, we examine the capabilities of our method for estimation of emissions of the proxy species by means of OSSEs. Specifically, we apply our method to synthetic "observational" data featuring known uncertainties that are evaluated by considering the misfits between real observation and corresponding simulated data. Specifically, to generate the synthetic data, we assumed that the covariances of cumulated errors in the real measurement and simulation data can be described by the three-dimensional covariance function, $\mathrm{cov}^s\left(\rho_x, \rho_y, \rho_t\right)$, that can be approximated as follows:

$$\mathrm{cov}^s\left(\rho_x, \rho_y, \rho_t\right) \cong \mathrm{cov}^s_x\left(\rho_x\right) \mathrm{cov}^s_y\left(\rho_y\right) \mathrm{cov}^s_t\left(\rho_t\right), \quad (16)$$

where ρ_x and ρ_y denote the distances between a pair of observations in west-to-east and south-to-north directions, respectively; ρ_t is the period (the lag) between different observations; and cov^s_x, cov^s_y, and cov^s_t are the respective one-dimensional covariance functions. We further approximated the covariance functions by using misfits between the observations and simulations as follows:

$$\mathrm{cov}^s_*\left(\rho_*\right) \sim \sum\nolimits_i \sum\nolimits_j H^s_{ij}[\rho_*] \left(C^s_{oi} - C^s_{mi} + \Delta^s_i\right)\left(C^s_{oj} - C^s_{mj} + \Delta^s_j\right), \quad (17)$$

where the subscript $*$ denotes either x, y, or t; $H^s_{ij}[\rho_*]$ is the selection operator which is nonzero (unity) only for those

pairs of data points that correspond to a given value of ρ_*; C^s_o and C^s_m are the vectors of the observational and simulated data; and $\mathbf{\Delta}^s$ is the bias. The distances and the lag were expressed in the numbers of grid cell and days, respectively. The vector $\boldsymbol{C}^s_o$ involved in Eq. (17) represents the actual observational data described in Sect. 2.1. The simulated data, $\boldsymbol{C}^s_m$, were obtained from the model base run results presented in Sect. 2.4, and the bias was evaluated on the monthly basis as the zero-order estimate obtained by applying Eq. (6) to the same data (that is, without using top-down emission estimates). The covariance functions, cov^s_x, cov^s_y, and cov^s_t, evaluated according to Eq. (17) were found to have the following characteristic scales (corresponding to a 2-fold decrease of the covariance functions): 3 (5) and 2 (3) grid cells and 1 (1) day in the case of NO_2 (CO) columns, respectively, although these scales do not necessarily reflect the presence of rather long "tails" in the covariance functions.

Our OSSEs are not expected to disregard any of possible errors in observational and model data that determine variability of the misfits between the observations and simulations within 1 month, although it should be noted that Eq. (16) provides a rather simplified temporal and special structure of such errors. In particular, our error model does not allow us to take into account probable error "clusters" that can be associated with the aggregation error in our optimal emission estimates, as well as less probable model errors (see Sect. 3.4) that affect the modeled relationship between the NO_x emissions and the NO_2 columns but do not contribute to the variability of the differences between the observations and simulations. Nonetheless, inversion of the synthetic data generated even with the simplified error model is useful, as it allows us to assess the adequacy of our uncertainty estimates obtained with the subsampling technique in the presence of probable covariances of errors in the input data, as well as to examine the self-consistency of our procedure (that is, to see whether or not any systematic deviations of our optimal emission estimates from the "true" emission values are covered by the corresponding confidence intervals).

Estimations given by Eqs. (16) and (17) were used to set up a Monte Carlo experiment in which the vector $\boldsymbol{C}^s_m$ (obtained either from the model base run or from a model run with the emissions perturbed as explained below) represented the true content of a given species, while the synthetic observations were generated by adding random errors (and, in some cases, biases) to $\boldsymbol{C}^s_m$. Samples of the errors with the covariance structure given by Eq. (16) were generated from a Gaussian distribution by using a standard method (Press et al., 1992) involving the Cholesky decomposition of the correlation matrices that were specified, in our case, using the covariance functions given by Eqs. (16) and (17). The Cholesky decomposition of a correlation matrix gives a lower-triangular matrix, $\mathbf{L}$; applying this matrix to a vector of uncorrelated samples of Gaussian noise, $\boldsymbol{u}$, gives a vector, $\mathbf{L}\boldsymbol{u}$, with the components satisfying the original correlation matrix. Using the synthetic data, we obtained uncertain emission estimates which were compared with true emission data specified in the model. Each Monte Carlo experiment included 100 iterations performed with the same covariance matrix and with the same bias, $\mathbf{\Delta}^s$, but with different samples of random errors. The bias added to $\boldsymbol{C}^s_m$ in each experiment for any given day was specified by linearly interpolating (in time) the monthly biases shown in Fig. 3c, d, with the magnitude of the monthly bias values scaled (in different experiments) with a factor (δ) ranging from 0 to 1.

The uncertainties (expressed as the standard error) in the emission estimates were evaluated both in the "direct" way (as the root mean square difference between the uncertain and true emission estimates) and by averaging squares of σ^s_c calculated by using the subsampling technique described above. The magnitude of errors in the synthetic data was changed in different experiments by applying a scaling factor (σ) ranging from 0 to 1 to the covariance matrix given by Eq. (16). An additional factor (ξ) was introduced to scale the non-diagonal components of the covariance matrix: ξ equals zero in an "ideal" case where errors in each grid cells and days are statistically independent from errors in any other grid cells and days. Along with the experiments where the "true" emissions were set to be exactly the same as the bottom-up emissions used in the base run of our model (see Figs. 6, 7), we performed the experiments where the base case emissions for both NO_x and CO were either uniformly increased by 20 % (see Fig. 8) or increased by 20 % only for the EHI categories but reduced by 20 % for the TCO category (see Fig. 9). Note that not only anthropogenic NO_x and CO emissions were perturbed in the corresponding model runs but also respective anthropogenic emissions of all other model species, including those of NMHCs.

The results of the OSSEs indicate, in particular (see Figs. 6, 7), that if errors in the input data for different grid cells and days were statistically independent ($\xi = 0$), the uncertainties (evaluated in the "direct" way with both σ and δ equal unity) of our top-down estimates of both NO_x and CO emissions would be very small, specifically 0.9 and 0.6 % for the NO_x emission estimates in the EHI and TCO sectors and somewhat larger (13 and 5 %) for the CO emission estimates for the same sectors. The fact that the uncertainties in our emission estimates remain rather small in spite of the large uncertainties in the input data (see Sect. 2.4) clearly indicates that the inverse problem considered is not ill conditioned. Expectedly, taking the error covariances into account increases the emission estimate uncertainties considerably. The uncertainties in the estimates of NO_x (CO) emissions from the EHI and TCO sectors are found to be 4 (28) and 5 (17) %, respectively. Larger uncertainty levels in the CO emission estimates compared to those in the NO_x emission estimates are an expected result, reflecting the fact that the constraints to CO emissions provided by the CO observations are much weaker than the corresponding constraints provided by the NO_2 observations to the NO_x emissions. In-

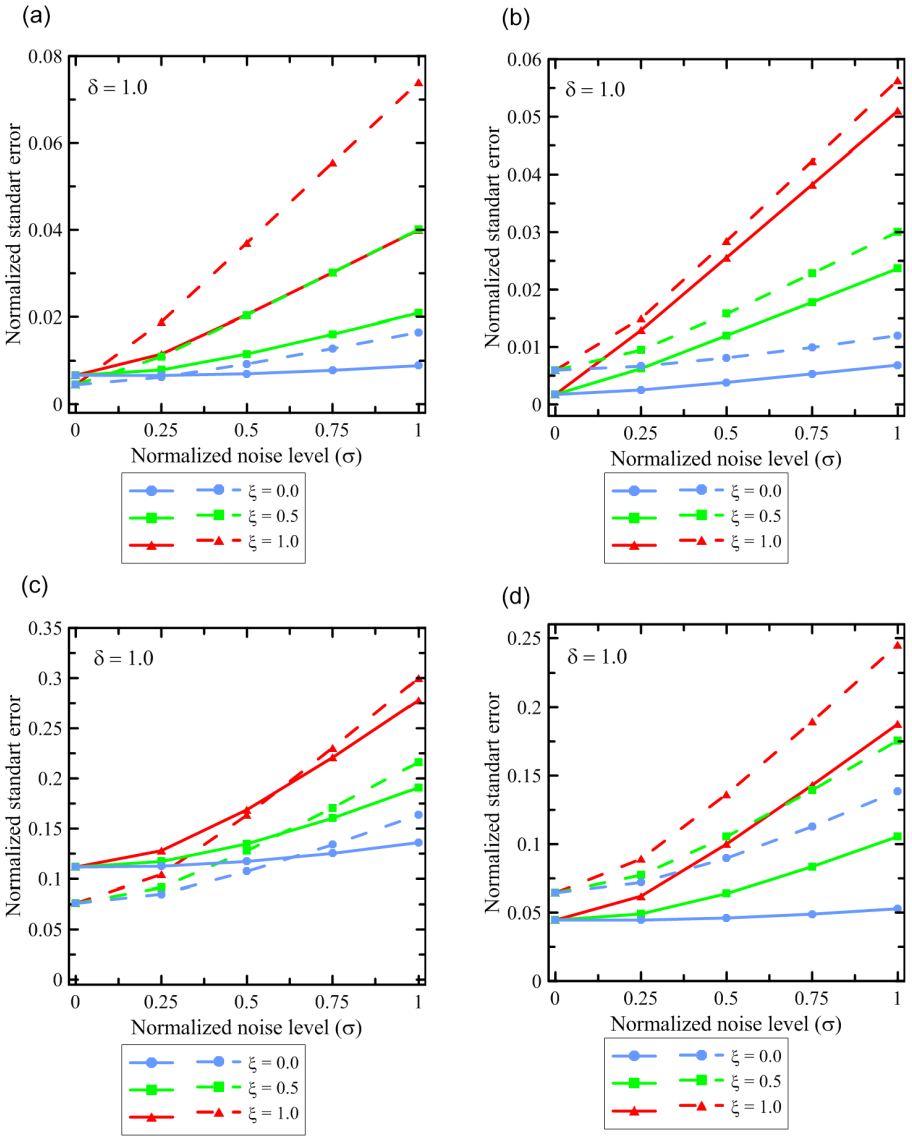

Figure 6. Results of the OSSEs for estimation of NO_x **(a, b)** and CO **(c, d)** emissions: the dependencies of the normalized standard error of the NO_x (CO) emission estimates for the EHI **(a, c)** and TCO **(b, d)** source categories on the level of noise (that is, on the value of the diagonal elements, σ, of the error covariance matrixes) in the input "synthetic" data. The noise level is normalized to its magnitude estimated with the real measurement and simulation data. Apart from the random noise, the synthetic data included the bias that was specified (for any given day) by linearly interpolating (in time) the monthly biases shown in Fig. 3c, d. Different colors show the results obtained with the different levels of error co-variances (ξ is the scaling factor applied to non-diagonal elements of the covariance matrix). The standard errors estimated in the "direct" way (as the RMSE representing the differences between the emission estimates inferred from the synthetic data and the "true" NO_x emission estimates) and by using the subsampling technique are shown by solid and dashed lines, respectively.

deed, an "emission signal" in the CO data considered (see Figs. 3 and 4) is, on average, much weaker than that in the NO_2 data; moreover, taking into account that the atmospheric lifetime of CO is much longer compared to that of NO_x, an emission signal from a given grid cell is effectively spread between a much larger number of grid cells (and days) in CO than in NO_2 observations, resulting in large non-diagonal elements of the Jacobian matrix and potentially leading to a stronger sensitivity of the CO emission estimates to errors in the input data. Interpretation of changes in the uncertainty estimates with respect to the ideal case is difficult: it can only be speculated that the increase in the uncertainties is larger in the NO_x than in CO emission estimates, probably because introduction of the error covariance is effectively equivalent to aggregation of available observations into a few "super-observations", leading to suppression of the effect of large non-diagonal elements in the Jacobian matrix describing the relationship between the CO emissions and observations.

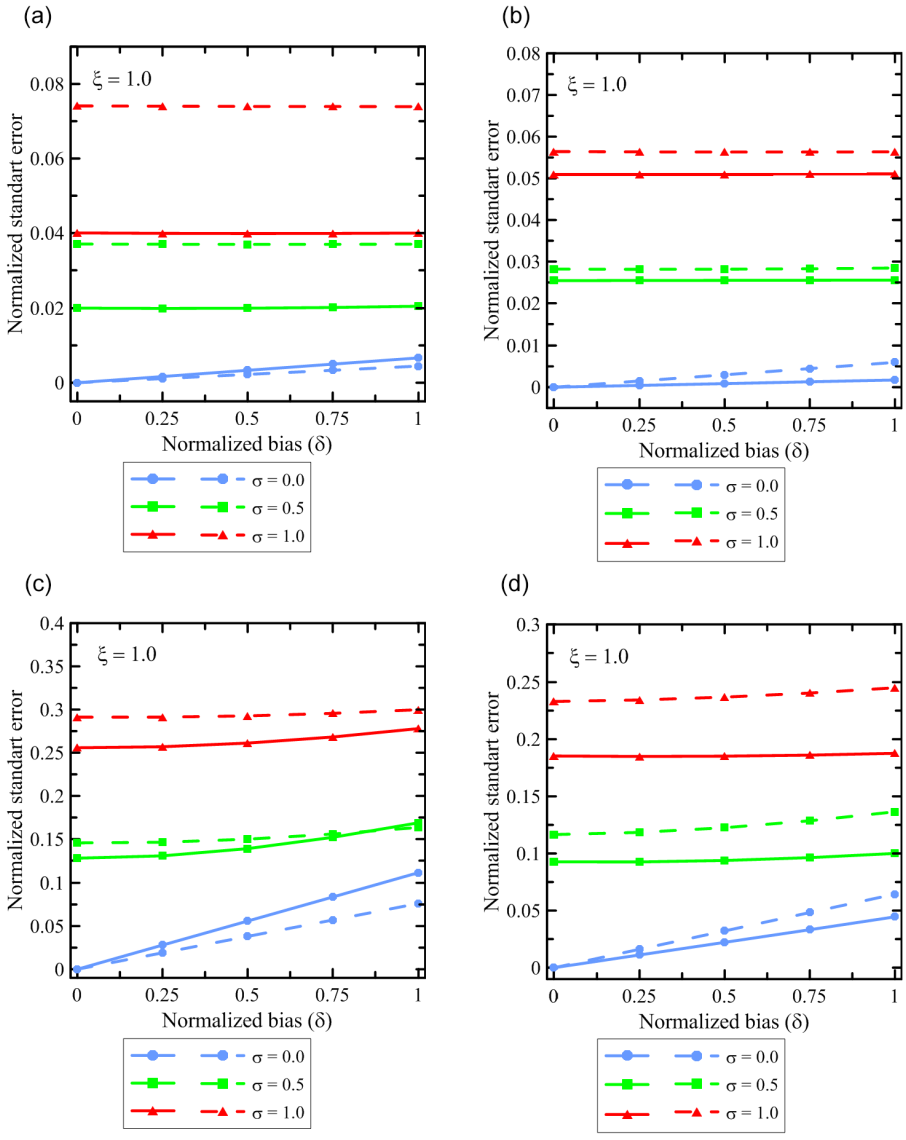

Figure 7. The same as in Fig. 6 but for the dependencies of the normalized standard error on the scaling factor, δ, characterizing the bias applied to the synthetic data (see Sect. 3.5 for further details).

Importantly, it is found that introduction of a bias into the synthetic data does not have a strong impact on the accuracy of the retrieved emission estimates (see Fig. 7) affected by random errors in the input data. This result confirms that our inverse modeling scheme is indeed capable of efficiently filtering out the bias, even if it is not constant during 1 month (as assumed in Eq. 6).

The results of our OSSEs also indicate that the subsampling technique employed in this study provides reasonable uncertainty estimates, although it tends to overestimate the actual uncertainties in the experiments representing the most realistic case (where all the scaling factors equal unity). We consider a probable overestimation of uncertainties in our emission estimates as a rather positive feature of our procedure, making conclusions of this study more reliable.

The results shown in Figs. 8 and 9 demonstrate that the optimal emission estimates obtained with our inversion procedure are likely not significantly biased even if the true emissions are considerably different from the bottom-up emission inventory data. These results also confirm that our inversion procedure enables efficient separation of the uncertainties in the model data due to emission errors from other systematic uncertainties in the model and observation data. Importantly, the fact that the emissions perturbations are retrieved almost perfectly indicates that the effects of chemical interactions (nonlinearities) and changes in NMHC emissions on the relationships between NO_x and CO emissions and the NO_2 and

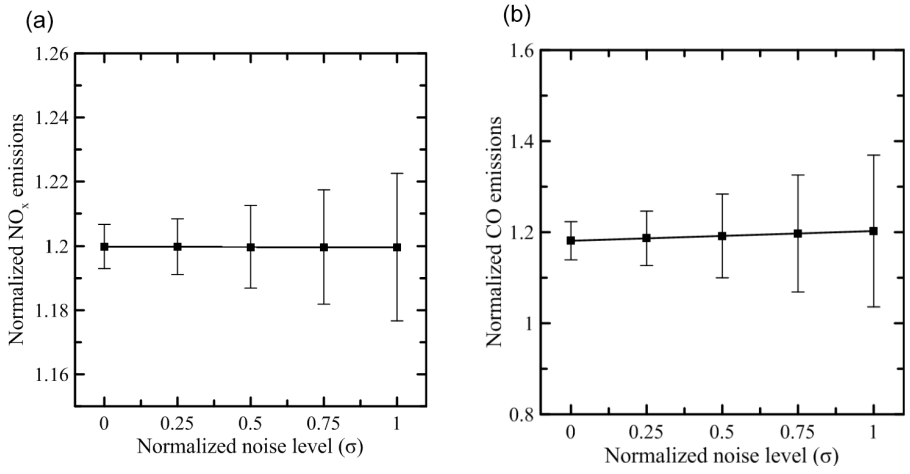

Figure 8. The total NO_x **(a)** and CO **(b)** emission estimates ($\hat{E}^{s}_{tot}$) obtained in the OSSEs where the "true" emissions were specified by scaling the bottom-up emissions (employed in the base case model run) with the factor of 1.2. The emission estimates (normalized to the respective bottom-up emission estimates, $\widetilde{E}^{s}_{tot}$, based on the EMEP inventory data) represent the average over the ensemble of 100 Monte Carlo experiments, each with a different sample of noise in the synthetic data, and are shown as a function the noise level (σ). Both non-diagonal elements of the error co-variance matrix and the systematic uncertainties were taken into account in the OSSEs (specifically, both ξ and δ were set to be equal to unity; see further details in Sect. 3.5). Note that the value of 1.2 on the axis of ordinates corresponds to a perfect emission estimate in the case considered. Note also that the confidence intervals shown were estimated by using the subsampling technique (see Eq. 12) that is expected to predict a nonzero uncertainty (associated with the bias estimation procedure) even when the synthetic input data are not affected by random uncertainties (that is, when $\sigma = 0$; see also blue lines in Fig. 7).

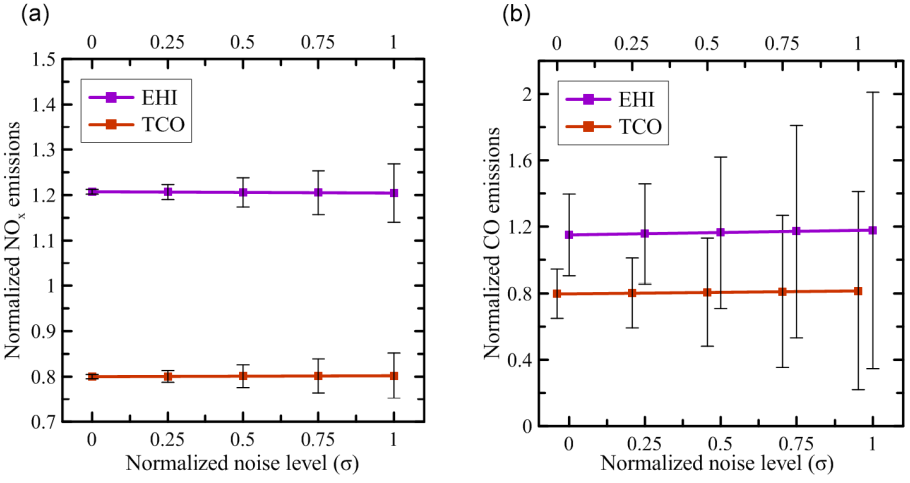

Figure 9. The NO_x **(a)** and CO **(b)** emission estimates obtained similarly to the estimates shown in Fig. 8 but separately for the two source categories (EHI and TOC) in the OSSEs, where the "true" emissions in the EHI and TCO were specified by scaling the corresponding bottom-up emissions (employed in the base case model run) with the factors of 1.2 and 0.8. Note that the estimates for the EHI and TCO categories are depicted by using the abscissa axes at the bottom and at the top of the plots, respectively.

CO columns, respectively, are likely rather small in the situation considered, although it should be noted that such effects can be stronger if the differences between the bottom-up and true emissions were much larger than in our experiments (±20 %).

4 Results

4.1 NO_x and CO emission estimates

The estimates of anthropogenic NO_x and CO emissions from the EHI and TCO categories ($\hat{E}^{s}_{c}$) as well as from all sources aggregated together ($\hat{E}^{s}_{tot}$) based on actual observations are presented in Fig. 10. The corresponding numbers are listed

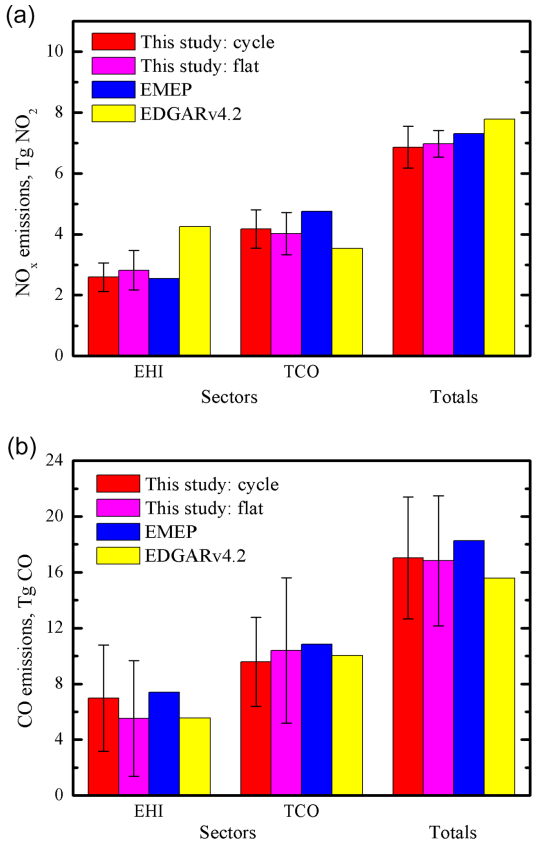

Figure 10. Top-down estimates ($\hat{E}^{s}_{c}$ and $\hat{E}^{s}_{tot}$) of the anthropogenic NO_x **(a)** and CO **(b)** emissions in the study region in comparison with the corresponding estimates from the EMEP and EDGAR v4.2 inventories. Our estimates are shown for the two cases ("cycle" and "flat") with different seasonal cycles of anthropogenic emissions.

in Table 1, which also shows alternative estimates ($\hat{E}^{s}_{sum}$) of the total emissions. The results are reported for the two estimation cases (cycle and flat; see Sect. 3.4) that involve different seasonal variations of anthropogenic emissions in the model (specifically, the seasonal cycles specified in the standard version of the CHIMERE CTM were used for the cycle case estimations, while constant monthly anthropogenic emissions with diurnal and weekly variations were employed for the flat case). Note that the flat case is obviously unrealistic and is considered here only for testing purposes; accordingly, if not stated otherwise, below we discuss estimates obtained for the main (cycle) case. The uncertainties are reported in terms of the 68.3 % (1σ) confidence intervals. It should be noted that the confidence intervals were evaluated under the assumption (see Sect. 3.4) that the NO_x and CO emission estimates are not significantly affected by any systematic errors that cannot be manifested in the differences between the emission estimates for different subregions and seasons. If this assumption holds, the uncertainty intervals evaluated with our subsampling technique may actually correspond to a higher confidence level, as discussed in Sect. 3.4 and 3.5.

All of our optimal (top-down) estimates of both the total NO_x and CO emissions are slightly (less than 10 %) smaller than the bottom-up estimates based on the EMEP inventory data; the differences between the top-down and bottom-up estimates are not statistically significant. The relative uncertainties in our estimates of the total emissions range from 10 % (in case of the $\hat{E}^{s}_{tot}$ estimate for the NO_x emissions) to 30 % (in case of the $\hat{E}^{s}_{sum}$ estimate for the CO emissions). A low uncertainty in our estimate of the total NO_x emissions is not surprising, as random uncertainties of a very large number of individual retrievals used in our inverse modeling analysis tend to compensate each other, while systematic errors were taken into account in the framework of our inversion procedure explicitly. Nonetheless, this low uncertainty estimate should be considered with a certain degree of caution as it may not fully account for some unknown errors depending on emissions themselves (e.g., due to uncertainties in a model chemical scheme; see also Sect. 3.4). Taking into account our preliminary analysis (see Sect. 2.4) indicating that the contribution of the anthropogenic CO emissions in the study region into the corresponding CO columns is relatively small and the results of the OSSEs (see Sect. 3.5), it is also not surprising that the uncertainties in our CO emission estimates are much larger than those in the NO_x emission estimates.

The differences between our alternative estimates of the total emissions, $\hat{E}^{s}_{sum}$ and $\hat{E}^{s}_{tot}$, are also small compared to the uncertainties of those estimates, while the uncertainties in $\hat{E}^{s}_{sum}$ are larger than the uncertainties in $\hat{E}^{s}_{tot}$. The difference between the uncertainties in $\hat{E}^{s}_{sum}$ and $\hat{E}^{s}_{tot}$ would be difficult to predict a priori, particularly because the cost function (see Eq. 4) employed in this study includes the bias whose estimation may increase uncertainties in the emission estimates to a various extent, depending on the number of variables to be optimized. Our emission estimates for the individual source categories are much more uncertain than the estimates of the total emissions: the uncertainties range from 15 % in the case of the NO_x emission estimate for the TCO sector up to 54 % in the case of the CO emission estimate for the EHI sector. The absolute differences of our estimates of both CO and NO_x emissions with the EMEP data are smaller than the respective uncertainty range. It may be noteworthy that our estimates for both the CO and NO_x emissions from the TCO sector are $\sim$ 12 % lower than the corresponding EMEP estimates. This observation indicates that there may be a common bias in the EMEP data for both NO_x and CO emissions in this sector; however, available information does not allow us to make a firmer conclusion in this regard.

Unlike the EMEP data, the EDGAR v4.2 data strongly disagree with our estimate for the NO_x emissions from the EHI sector. The differences of our estimates with the EDGAR v4.2 data are also larger than with the EMEP data

Table 1. The optimal estimates of the anthropogenic NO_x and CO emissions (Tg NO_2 and Tg CO, respectively) from the study region. The numbers in brackets represent the one-sided 68.3 % confidence intervals (in % relative to the respective optimal estimate).

	Estim.	EHI			TCO			Totals			
Species	case	$\hat{E}_1^s$	EMEP	EDGAR	$\hat{E}_2^s$	EMEP	EDGAR	$\hat{E}_{sum}^s$	$\hat{E}_{tot}^s$	EMEP	EDGAR
NO_x	cycle	2.59 (18)	2.55	4.25	4.17 (15)	4.75	3.53	6.76 (11)	6.86 (10)	7.30	7.78
	flat	2.82 (23)			4.02 (17)			6.84 (7)	6.97 (7)		
CO	cycle	6.99 (54)	7.41	5.55	9.59 (33)	10.84	10.02	16.57 (30)	17.03 (26)	18.25	15.57
	flat	5.53 (75)			10.4 (50)			15.93 (25)	16.82 (28)		

in particular in the cases of the $\hat{E}_{tot}^s$ estimates of both NO_x and CO emissions and in the case of CO emission estimate for the EHI sector, although smaller in the cases of the CO emission estimates in the TCO sectors. It is noteworthy that the differences between all our NO_x emission estimates with the corresponding EDGAR data are statistically significant. In general, our analysis indicates that the NO_x and CO emission data provided by the EMEP inventory are more consistent with the NO_2 and CO satellite measurements than those given by the EDGAR v4.2 inventory. This is an expected result because the methodology used in the EMEP inventory is specific to national statistical data available from European countries, while the EDGAR v4.2 inventory uses another approach which is deemed to be robust at the global scale.

The differences between the estimates obtained with different types of seasonal variations of anthropogenic emissions are small compared to the uncertainty in the estimates for the cycle case, although not entirely negligible. Evidently, these differences cannot explain the significant disagreement of our NO_x emission estimates with the EDGAR v4.2 data. Nonetheless, our test results indicate that the effect of possible inaccuracies in the seasonal variations of emissions may not be negligible and should not be disregarded a priori when examining the significance of the differences between the top-down estimates of annual emissions and respective bottom-up inventory data. Note that the uncertainties in the NO_x and CO emission estimates for the individual source categories tend to be larger for the flat case than for the cycle case, while, in contrast, the uncertainties in the total NO_x emission estimates are larger for the cycle case. Such nonsymmetrical differences indicate that none of the cases considered represent the seasonal cycles in NO_x and CO emissions quite perfectly.

The uncertainty levels in our estimates of both NO_x and CO emissions using actual data are considerably larger than those obtained above in our OSSEs (see Sect. 3.5) in which synthetic data were generated using a simplified error model. (Note that to be compared with the confidence intervals discussed in this section the standard errors presented in Sect. 3.5 should be multiplied with the t score of about 1.2.) This result indicates that, as expected, the uncertainties in our emission estimates are caused not only by random uncertainties in the input (measurement and simulation) data but also by other factors – such as the aggregation error and spatial variability of the bias – which could not be adequately taken into account in our tests. Besides, the actual temporal and spatial structure of both the model and measurement errors is likely much more complex and irregular than that assumed in Eq. (16). Anyway, unless the data subsamples defined in Sect. 3.5 are strongly affected by temporal and spatial covariances of errors in the input data (as evidenced by our OSSEs, that is unlikely the case in this study), the confidence intervals provided by the subsampling technique are expected to be sufficiently reliable even in such a complex real situation as that considered in this study.

Note that the uncertainties of our top-down estimates of NO_x emissions in the region considered turned out to be comparable with the differences between similar estimates provided by different emissions inventories, or even smaller than them. Therefore, our top-down NO_x emission estimates can be considered as an independent alternative to bottom-up estimates based on emission inventory data alone. Both our NO_x and CO emission estimates could formally be combined (in the Bayesian way) with the bottom-up (a priori) estimates; the uncertainties in the combined (a posteriori) estimates would probably be lower than the uncertainties in either the top-down or a priori estimates taken alone.

In general, our results confirm the findings of previous studies (see the corresponding references in Introduction) showing that NO_2 and CO retrievals from satellite measurements can provide useful information on NO_x and CO emissions over high emission regions. In this regard, it can be noted that while previous inverse modeling studies utilized satellite CO measurements to estimate CO emissions from regions with predominantly anthropogenic sources involved global CTMs (e.g., Pétron, 2004; Fortems-Cheiney et al., 2009; Kopacz et al., 2010; Jiang et al., 2015), we obtained reasonable top-down CO emission estimates by using a regional model. We regard this fact as a promising development, because the use of regional models (usually featuring a higher spatial resolution than global CTMs and employing high-resolution regional emission inventories that are likely more accurate and detailed compared to global ones) in inverse modeling procedures can, potentially, provide more detailed and accurate constraints to CO emissions from various sources. A major difficulty that needs to be overcome in ap-

Table 2. The NO_x-to-CO_2 ($g\,CO_2\,[g\,NO_2]^{-1}$) and CO-to-CO_2 ($g\,CO_2\,[g\ CO]^{-1}$) emission conversion factors based on the EDGAR v4.2 emission inventory along with their relative uncertainties given in brackets as one-sided 68.3 % confidence interval (in %).

Sectors	NO_x-to-CO_2	CO-to-CO_2
EHI	494.97 (58)	378.63 (38)
TCO	262.06 (30)	92.42 (22)
TOT	389.22 (4)	194.50 (22)

plications of a regional CTM for estimating anthropogenic CO emissions by inverse modeling is associated with probable biases in boundary conditions, especially for CO, which has a long chemical lifetime compared to the transit time across the European domain; here we tackled this difficulty by means of a special procedure aimed at eliminating systematic differences between the measured and simulated data. The results of the OSSEs presented in Sect. 3.5 (see Figs. 8, 9) indicate that our estimation procedure successfully relies on the spatial gradients of CO (and NO_2) columns within the European domain to constrain the CO (and NO_x) emissions rather than on the average abundance (which is strongly driven by the boundary conditions) in the measurements.

4.2 Fossil-fuel CO_2 emission estimates

Our hybrid FF CO_2 emission estimates presented in this section were obtained by applying the conversion factor values listed in Table 2 to our top-down estimates of NO_x and CO emissions discussed above. The FF CO_2 emission estimates derived from NO_2 and CO measurements ($\hat{E}^{CO_2}_{sc}$ and $\hat{E}^{CO_2}_{s,\,tot}$) as well as the combined FF CO_2 emission estimates ($\hat{E}^{CO_2}_{comb,\,c}$ and $\hat{E}^{CO_2}_{comb,\,tot}$) are shown in Fig. 11 in comparison with the corresponding data of emission inventories. The same estimates are listed in Table 3, which, in addition, presents another version of the hybrid estimates of total FF CO_2 emissions, $\hat{E}^{CO_2}_{s,\,sum}$ and $\hat{E}^{CO_2}_{comb,\,sum}$ (see Sect. 3.3). Note again (see also Sect. 2.3) that CO_2 emissions from the cement production are not included in our estimates. Two types of the confidence intervals are provided along with the CO_2 emission estimates based on measurements of one proxy species. The full confidence intervals include the uncertainty in the top-down estimates of the proxy species as well as the uncertainty in the conversion factors. The partial confidence intervals were estimated by taking into account only the uncertainty in the top-down estimates of the NO_x and CO emissions.

The relative differences of NO_2- or CO-measurement-based FF CO_2 emission estimates with the EDGAR v4.2 CO_2 data correspond to the differences of our top-down NO_x or CO emission estimates with the EDGAR v4.2 data for the respective species. This is not surprising, as the con-

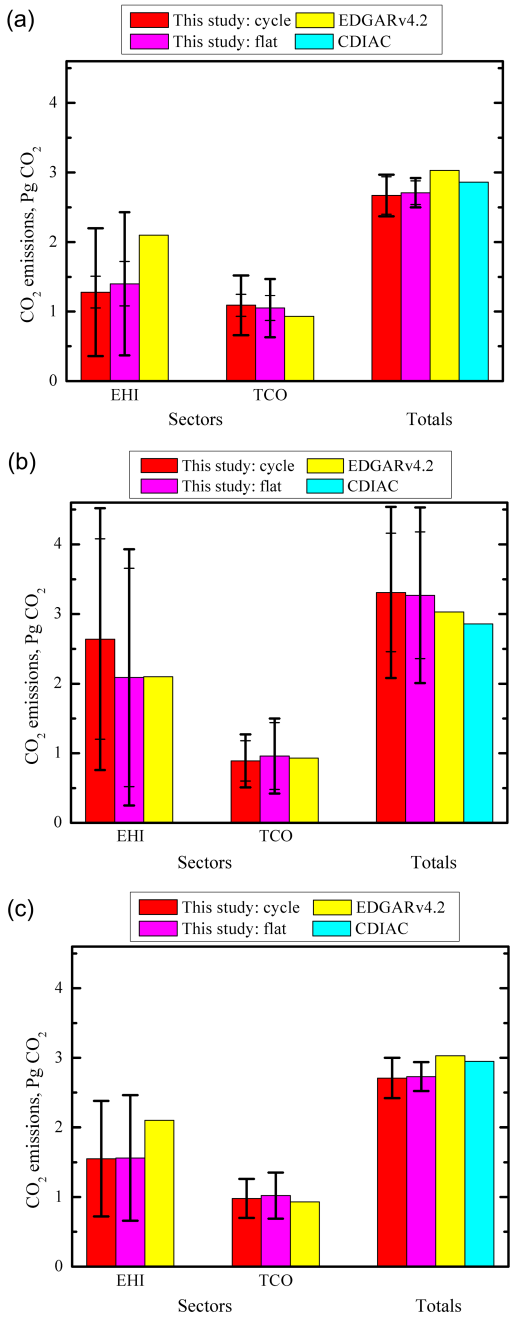

Figure 11. Hybrid estimates of the fossil-fuel CO_2 emissions ($\hat{E}^{CO_2}_{sc}$, $\hat{E}^{CO_2}_{s,\,tot}$ $\hat{E}^{CO_2}_{comb,\,c}$, and $\hat{E}^{CO_2}_{comb,\,tot}$) from the study region in comparison with the data of the EDGAR v4.2 and CDIAC emission inventories. The estimates were obtained either from **(a)** only NO_x and **(b)** only CO or **(c)** from both NO_x and CO measurements. The "partial" and "full" 68.3 % confidence intervals are also shown: the partial intervals (depicted by narrow brackets and not shown for the combined CO_2 emission estimates) are determined only by uncertainties in the top-down estimates of NO_x or CO emissions, while the full intervals also take into account probable uncertainties in the conversion factors.

Table 3. The estimates of the fossil-fuel CO_2 emissions ($Pg\,CO_2$) from the study region in comparison with corresponding data (when available) of the EDGAR v4.2 and CDIAC emission inventories. The numbers in brackets represent the one-sided 68.3 % confidence intervals (in % relative to the respective optimal estimate). Along with the "full" confidence intervals, the "partial" confidence intervals are shown after a slash (except for the combined estimates) and do not include uncertainties in the conversion factors.

Inversion	Estim.	EHI		TCO		Totals			
settings	case	$\hat{E}^{CO_2}_{s,1}$	EDGAR	$\hat{E}^{CO_2}_{s,2}$	EDGAR	$\hat{E}^{CO_2}_{s,sum}$	$\hat{E}^{CO_2}_{s,tot}$	CDIAC	EDGAR
NO_x-based	cycle	1.28 (72/18)	2.10	1.09 (39/15)	0.93	2.37 (43/12)	2.67 (11/10)	2.86	3.03
	flat	1.40 (74/23)		1.05 (40/17)		2.45 (44/9)	2.71 (8/7)		
CO-based	cycle	2.64 (71/55)		0.89 (42/33)		3.53 (49/35)	3.31 (37/26)		
	flat	2.09 (88/75)		0.96 (57/50)		3.06 (54/42)	3.27 (38/28)		
NO_x- and	cycle	1.55 (54)		0.98 (29)		2.67 (33)	2.71 (11)		
CO-based	flat	1.56 (57)		1.02 (33)		2.63 (34)	2.73 (8)		

version factors relating CO_2 emissions with the respective proxy species were based on the EDGAR v4.2 inventory. The full relative uncertainties in our CO_2 emission estimates are larger than the uncertainties in our estimates of emissions of proxy species due to uncertainties in the conversion factors. Among the uncertainties in the conversion factors, σ^{F}_{sc}, they are largest for the NO_x-to-CO_2 and CO-to-CO_2 emission conversion factors for the EHI source category (58 and 38 %, respectively).

These uncertainties strongly contribute to the confidence intervals of the respective CO_2 emission estimates. In contrast, the uncertainties are relatively small in the NO_x-to-CO_2 and CO-to-CO_2 emission conversion factors for the total emissions (4 and 22 %, respectively); those uncertainties contribute considerably to the full confidence intervals only for the total CO_2 emission estimates based on the CO measurements, while the uncertainty in the respective NO_2-measurement-based estimate is mostly due to the uncertainty in the top-down NO_x emission estimates. Note that as discussed in Sect. 3.4 and 3.5 our method is likely to overestimate uncertainties in both the top-down estimates and in the conversion factors.

Taking into account the full confidence intervals (which are, in some cases, very wide), all our estimates are in agreement with the EDGAR v4.2 data, except for the estimates of the total CO_2 emissions ($\hat{E}^{CO_2}_{s,tot}$) based on NO_2 measurements and on both NO_2 and CO measurements. Our hybrid NO_2-measurement-based and combined estimates of the total CO_2 emissions (2.67 and 2.71 $Pg\,CO_2$ with the relative uncertainties of about 10 %) are 12 and 11 % lower than the EDGAR v4.2 estimate (3.03 $Pg\,CO_2$), respectively. These differences are statistically significant but at the edge of significance with the given confidence level. Note that while discussing statistical significance of the differences between the hybrid and bottom-up emission estimates, we do not take into account the uncertainty in the bottom-up inventory data, which has not been reported. The differences between the same hybrid estimates and the corresponding estimate (2.86 $Pg\,CO_2$) provided by the CDIAC inventory (7 and 5 %) are slightly smaller than the differences with the EDGAR v4.2 data and are not statistically significant. Therefore, our analysis suggests that the CO_2 emissions in the region considered are likely estimated more accurately by CDIAC than by EDGAR v4.2; however, the difference between the data of the two inventories in the case considered is small (~ 6 %).

Note that if the conversion factor uncertainties were not taken into account, which is not recommended, the difference between our NO_2-measurement-based CO_2 emission estimate for the EHI sector and the respective EDGAR v4.2 estimate would be statistically significant. However, it is not significant with respect to the full confidence interval. Considering the emission estimates for the EHI sector along with the total CO_2 emission estimates illustrates a possible way of using our method for evaluation of bottom-up FF CO_2 emission inventory data. That is, assuming that the confidence intervals for our estimates are sufficiently reliable, we can argue that a difference between hybrid and bottom-up estimates that exceeds uncertainties associated with measurement and model errors may, in a general case, be due to the two following reasons: (1) there are inconsistencies between bottom-up estimates of emissions of CO_2 and of a corresponding proxy species or/and (2) a bottom-up CO_2 emission estimate is inaccurate. Taking uncertainties in the conversion factors into account allows examination of the first reason: evidently, it cannot be ruled out in the case of the emission estimates for the EHI sector. However, the first reason alone is not sufficient to fully explain the differences between the hybrid and bottom-up estimates of the total CO_2 emissions.

Comparing NO_2- and CO-measurement-based CO_2 emission estimates (which, ideally, should be the same) enables their cross-validation. All kinds of NO_2-measurement-based CO_2 emission estimates are found to be consistent with the respective CO-measurement-based estimates in the sense that their confidence intervals are intersecting. In principle, this is an important result confirming that uncertainties in our emission estimates are not underestimated, since NO_2 and CO measurements are independent from each other. However, it should be noted that the uncertainties in CO-

measurement-based estimates are so large that such estimates can hardly be useful as a unique source of information on CO_2 emissions. Similar large uncertainties are associated with NO_2-measurement-based CO_2 emission estimates for the EHI and TCO sectors, as well as with the total CO_2 emission estimates obtained by summing the NO_2-measurement-based estimates for the individual sectors together. While the uncertainties in the CO-measurement-based estimates are mostly caused by uncertainties in the top-down estimates of CO emissions, the uncertainties in the NO_2-measurement-based estimates are mainly associated with uncertainties in the conversion factors.

Importantly, the combined estimates (based on both NO_2 and CO measurements) of the FF CO_2 emissions from individual sectors feature considerably lower relative uncertainties (evaluated with Eq. 11) than the uncertainties in the estimates based on measurements of only one proxy species (for example, relative uncertainties of 39 and 42 % for the NO_2- and CO-measurement-based estimates, respectively, are reduced to a relative uncertainty of 29 % in the combined estimate for the TCO sector). This fact illustrates the potential usefulness of combining hybrid estimates based on independent measurements of different proxy species such as NO_2 and CO. The uncertainty of our combined estimate $\left(\hat{E}^{CO_2}_{comb,\,tot}\right)$ of the total CO_2 emissions is very insignificantly smaller than the uncertainty of the corresponding NO_2-measurement-based estimate.

As mentioned in Sect. 3.3, the uncertainty intervals for our combined estimates evaluated with Eq. (11) can be reliable only if the hybrid emission estimates derived from measurements of individual species are statistically independent. We believe that the CO_2 emission estimates derived from NO_2 and CO measurements are indeed sufficiently independent particularly because NO_2 (as a part of the NO_x chemical family) and CO experience very different atmospheric processing. Indeed, while the key role in spatial and temporal variations of CO is played by the transport processes (and boundary conditions in simulations), atmospheric evolution of NO_2 is very strongly affected by local photochemistry. Furthermore, the results of our estimations for the cycle and flat cases (see Table 1) indicate that probable errors in the seasonal cycles of the NO_x and CO emissions are also unlikely to result in considerable and common biases in the NO_x and CO emission estimates. Thus it seems reasonable to believe that possible model errors for these species are, for the most part, different in origin and weakly correlated. Any significant covariance of errors in CO and NO_2 measurement data is also hardly possible, as those measurements are performed with different satellite instruments and by using different methods (see Sect. 2.1). The covariance of errors in the conversion factors F^s_c for the different species is likely small, too (given the complexity of data involved in bottom-up estimates of different proxy species and the fact that NO_x and CO emissions depend on different technological factors and end-of-pipe measures), although we could not evaluate it confidently with available information. Therefore, the uncertainties in our combined emission estimates are based on an (so far) inevitable assumption that errors in the conversion factors for the different proxy species are statistically independent.

As in the case with the top-down estimates of NO_x and CO emissions, our hybrid estimates of FF CO_2 emissions are rather insensitive to the changes in simulations associated with using different seasonal cycles (cf. the estimates for the cycle and flat cases). That is, we can conclude that the impact of uncertainties in the assumed seasonal cycles of anthropogenic emissions on our hybrid estimates is small. In particular, such uncertainties can hardy explain the rather considerable difference between our "combined" estimate of the total CO_2 emissions and the corresponding estimate based on the EDGAR v4.2 inventory.

5 Summary and conclusions

We examined feasibility of estimation of FF CO_2 emissions by using NO_2 and CO column retrievals from satellite measurements. FF CO_2 emissions are an important component of the global carbon balance and are believed to be a major contributor to global warming. Although such emissions are usually known with better certainty than CO_2 fluxes associated with the biosphere, there still exist considerable divergences between data of different bottom-up FF CO_2 emission inventories; typically, such data cannot be evaluated by using atmospheric CO_2 measurements and rarely come with a reported uncertainty structure.

We followed the concept of proxy species that suggests constraining FF CO_2 emissions by using atmospheric measurements of minor species co-emitted with CO_2. We developed a general inverse modeling method aimed at estimation of the budgets of FF CO_2 emissions from different sectors of economy in a given region by using satellite measurements of proxy species. The method involves (1) obtaining top-down estimates of anthropogenic emissions for a proxy species from the satellite measurements and simulations performed with a mesoscale CTM, (2) using bottom-up emission inventories to relate CO_2 emissions with emissions of the proxy species, and (3) combining CO_2 emission estimates derived from measurements of different proxy species. Important parts of our method are robust techniques to estimate systematic differences between the measured and simulated data, as well as uncertainties in top-down estimates of the proxy species.

Considering NO_2 and CO as the proxy species, the method was applied to a western European region including 12 countries by using the NO_2 and CO column amounts retrieved from, respectively, the OMI and IASI satellite measurements along with the simulated data from the CHIMERE CTM. The study region was selected by taking into account that uncertainties in available bottom-up emission inventory data

for the EU countries with well-developed statistics are likely rather low, compared to potential uncertainties in FF CO_2 emission data for countries with less developed statistical infrastructure, although such uncertainties are likely not quite negligible even in the study region. The relationship between FF CO_2 emission and the NO_x and CO emissions was represented by the NO_x-to-CO_2 and CO-to-CO_2 emission conversion factors evaluated with the EDGAR v4.2 emission inventory. The estimates were obtained for the total FF CO_2 emissions from the region considered as well as individually for FF CO_2 emissions aggregated into two different source categories (sectors), such that the first category (EHI included the emissions associated mostly with energy and heat production and heavy industries, and the second category (TCO) comprised transport, chemical industry, and all other anthropogenic sources. Our FF CO_2 emission estimates were compared with the corresponding data of the EDGAR v.4.2 global emission inventory; in addition, our total FF CO_2 emission estimates for the study region were compared with the data of the CDIAC FF CO_2 emission inventory. The top-down estimates of NO_x and CO emissions were compared with the respective data from the European EMEP and global EDGAR v.4.2 emission inventories.

As expected (taking into account findings of several previous studies), the NO_2 column retrievals from OMI measurements provide rather strong constraints to NO_x emissions. Our most reliable top-down estimate of the total NO_x emissions is found to be only insignificantly (by about 6 %) lower than the respective bottom-up estimate based on the EMEP emission inventory; our estimates for the emissions from the EHI and TCO having much larger uncertainties (of about 18 and 15 %, respectively) are also found to agree with the corresponding estimates based on the EMEP emission inventory within the uncertainty range. Larger and statistically significant differences are found between our NO_x emission estimates and the respective data of the EDGAR v4.2 global emission inventory. In particular, our results suggest that the total NO_x emissions from the study region may be overestimated in the EDGAR v4.2 inventory by ~ 13 %, while the EDGAR emissions for the EHI sector are likely overestimated by more than 60 % (relative to our estimates).

In contrast to the NO_x emission estimates, our top-down estimates of the CO emissions are fully consistent with both the EMEP and EDGAR v4.2 emission data; however, this consistency is partly due to much larger uncertainties in our CO emission estimates (compared to uncertainties in the NO_x emission estimates). The relatively large uncertainties in the top-down CO emission estimates (~ 55 and ~ 35 % in the estimates for the EHI and TCO sectors, respectively, and ~ 25 % in the total CO emission estimate) are not surprising in view of the much lower sensitivity of the satellite CO measurements to anthropogenic CO emissions in the study region compared to the sensitivity of the NO_2 measurements to the anthropogenic NO_x emissions. Nonetheless, in spite of the large uncertainties (which may be overestimated by our procedure), the differences between our top-down estimates of CO emissions and respective EMEP data are rather small (less than 7 %). Similar to our NO_x emission estimates, the top-down CO emission estimates differ more considerably from the EDGAR v4.2 data.

The top-down estimates of the NO_x and CO emissions were used to obtain different hybrid estimates (combining different information coming from measurements and bottom-up inventories) of CO_2 emissions. The NO_2-measurement-based hybrid estimate of total CO_2 emissions is about 12 % smaller than the respective estimates based on the EDGAR v4.2; the difference exceeds the estimated uncertainty range (~ 11 %) of our estimate, although only marginally. In contrast, the difference between the same hybrid estimate and the corresponding estimate provided by the CDIAC inventory (~ 7 %) is not statistically significant. A large negative difference (more than 60 %) is found between our NO_2-measurement-based CO_2 emission estimate for the EHI source category and the corresponding EDGAR v4.2 estimate. This difference is, however, not statistically significant and can be mostly attributed to uncertainties in the NO_x-to-CO_2 emission conversion factor for the given source category. Our CO-measurement-based hybrid estimates of the total FF CO_2 emissions are larger than the respective bottom-up estimates based on both the EDGAR v4.2 and CDIAC data but the differences are not too big (less than 25 %) and can be well explained by uncertainties in our estimates. Similar to the case with the NO_2-measurement-based hybrid estimate, the largest difference between our CO-measurement-based FF CO_2 emission estimates and the EDGAR v4.2 data is found for the EHI source category, with our best estimate being about 26 % larger.

Taking into account the range of uncertainties, all our NO_2-measurement-based CO_2 emission estimates were found to be consistent with the respective CO-measurement-based estimates. This is an important result confirming the reliability of our approach. The combined emission estimates (based on both NO_2 and CO measurements) for individual source categories feature considerably smaller uncertainties than the corresponding partial estimates. Our combined estimate of total FF CO_2 emissions is weighed toward the NO_2-measurement-based estimate and is found to be ~ 11 and ~ 5 % lower than the respective estimates based on the EDGAR v4.2 and CDIAC data. The difference of our estimate with the EDGAR v4.2 data slightly exceeds the confidence interval of our combined estimate, while the difference with the CDIAC data is again not statistically significant.

In general, our analysis demonstrated that NO_2 and CO column retrievals from satellite measurements provide reasonable constraints to FF CO_2 emissions at the scale of western Europe. Although relative uncertainties in our top-down CO emission estimates were evaluated to be considerably larger than in the similar NO_x emission estimates based on NO_2 measurements, the CO column retrievals were found to be a useful source of independent information on FF

CO_2 emissions, particularly in the cases where probable uncertainties in the conversion factors for NO_x emissions are larger than uncertainties in the conversion factors for CO emissions. Differences between hybrid CO_2 emission estimates derived from the satellite data and respective estimates based on bottom-up emission inventory data can, in principle, be due to various kinds of uncertainties in the hybrid estimates (including uncertainties in the top-down estimates of NO_x and CO emissions and uncertainties in the conversion factors). We argue that such uncertainties can be roughly evaluated using the robust techniques described in this paper. Nonetheless, further research (involving, e.g., multi-model inversions and ensembles of independent emission inventories) is needed to ensure that the confidence intervals for the emission estimates actually take into account all possible estimation errors, including those associated with uncertainties in the modeled representation of chemical processes, in the boundary conditions for reactive species, and in the NO_x-to-CO_2 and CO-to-CO_2 emission conversion factors. Possible future developments of our approach can also include using NO_2 and CO retrievals from measurements performed by other satellite instruments (such as GOME-2, MOPITT and AIRS) together with the retrievals from the OMI and IASI measurements (as in this study), and implementing hybrid CO_2 emission estimates into a global transport model simulating CO_2 distribution in the atmosphere in order to validate them against ground-based and satellite CO_2 measurements. Finally, it should be noted that as FF CO_2 emission inventory data for the western European countries are likely much less uncertain than similar data for developing regions of the world, applications of our method to developing regions can be especially fruitful. In this regard, our method can become an integral part of a policy-relevant global carbon observing system (Ciais et al., 2014, 2015).

6 Data availability

The OMI and IASI retrievals are available at http://www.temis.nl/ (TEMIS, 2016) and http://ether.ipsl.jussieu.fr/ether/pubipsl/iasi_CO_uk.jsp (ESPRI, 2016), respectively. The EMEP, EDGAR v.4.2 and CDIAC emission inventory data are available at http://www.ceip.at/ms/ceip_home1/ceip_home/webdab_emepdatabase/emissions_emepmodels/ (EMEP/CEIP, 2014), http://edgar.jrc.ec.europa.eu/overview.php?v=42 (EC-JRC/PBL, 2011) and http://cdiac.ornl.gov/trends/emis/tre_coun.html (CDIAC, 2016). The modeled data used in this study are available upon request from the corresponding author, Igor Konovalov (konov@appl.sci-nnov.ru).

Acknowledgements. The study was supported by the Russian Science Foundation (grant no. 15-17-10024). We acknowledge the free use of tropospheric NO_2 column data from the OMI sensor from www.temis.nl and the use of CO column data from http://ether.ipsl.jussieu.fr/ether/pubipsl/iasi_CO_uk.jsp.

Edited by: Q. Zhang
Reviewed by: two anonymous referees

References

Akimoto, H., Ohara, T., Kurokawa, J., and Horii, N.: Verification of energy consumption in China during 1996–2003 by using satellite observational data, Atmos. Environ., 40, 7663–7667, doi:10.1016/j.atmosenv.2006.07.052, 2006.

Arellano Jr., A. F., Kasibhatla, P. S., Giglio, L., van der Werf, G. R., and Randerson J. T.: Top-down estimates of global CO sources using MOPITT measurements, Geophys. Res. Lett., 31, L01104, doi:10.1029/2003GL018609, 2004.

Baker, D. F., Law, R. M., Gurney, K. R., Rayner, P., Peylin, P., Denning, A. S., Bousquet, P., Bruhwiler, L., Chen, Y. H.,Ciais, P., Fung, I. Y., Heimann, M., John, J., Maki, T., Maksyutov, S., Masarie, K., Prather, M., Pak, B., Taguchi, S., and Zhu, Z.: TransCom3 inversion intercomparison: Impact of transport model errors on the interannual variability of regional CO_2 fluxes, 1988–2003, Global Biogeochem. Cy., 20, GB1002, doi:10.1029/2004gb002439, 2006.

Basu, S., Miller, J. B., and Lehman, S.: Separation of biospheric and fossil fuel fluxes of CO_2 by atmospheric inversion of CO_2 and $^{14}CO_2$ measurements: Observation System Simulations, Atmos. Chem. Phys., 16, 5665–5683, doi:10.5194/acp-16-5665-2016, 2016.

Berezin, E. V., Konovalov, I. B., Ciais, P., Richter, A., Tao, S., Janssens-Maenhout, G., Beekmann, M., and Schulze, E.-D.: Multiannual changes of CO_2 emissions in China: indirect estimates derived from satellite measurements of tropospheric NO_2 columns, Atmos. Chem. Phys., 13, 9415–9438, doi:10.5194/acp-13-9415-2013, 2013.

Boden, T. A., Marland, G., and Andres, R. J.: Global, Regional, and National Fossil-Fuel CO_2 Emissions, Carbon Dioxide Information Analysis Center, Oak Ridge National Laboratory, US Department of Energy, Oak Ridge, TN, USA, doi:10.3334/CDIAC/00001_V2012, 2011.

Boersma, K. F., Eskes, H. J., Veefkind, J. P., Brinksma, E. J., van der A, R. J., Sneep, M., van den Oord, G. H. J., Levelt, P. F., Stammes, P., Gleason, J. F., and Bucsela, E. J.: Near-real time retrieval of tropospheric NO_2 from OMI, Atmos. Chem. Phys., 7, 2103–2118, doi:10.5194/acp-7-2103-2007, 2007.

Boersma, K. F., Eskes, H. J., Dirksen, R. J., van der A, R. J., Veefkind, J. P., Stammes, P., Huijnen, V., Kleipool, Q. L., Sneep, M., Claas, J., Leitão, J., Richter, A., Zhou, Y., and Brunner, D.: An improved tropospheric NO_2 column retrieval algorithm for the Ozone Monitoring Instrument, Atmos. Meas. Tech., 4, 1905–1928, doi:10.5194/amt-4-1905-2011, 2011.

Bovensmann, H., Buchwitz, M., Burrows, J. P., Reuter, M., Krings, T., Gerilowski, K., Schneising, O., Heymann, J., Tretner, A., and Erzinger, J.: A remote sensing technique for global monitoring of power plant CO_2 emissions from space and related applications, Atmos. Meas. Tech., 3, 781–811, doi:10.5194/amt-3-781-2010, 2010.

Bréon, F. M., Broquet, G., Puygrenier, V., Chevallier, F., Xueref-Remy, I., Ramonet, M., Dieudonné, E., Lopez, M., Schmidt, M., Perrussel, O., and Ciais, P.: An attempt at estimating Paris area CO_2 emissions from atmospheric concentration measurements,

Atmos. Chem. Phys., 15, 1707–1724, doi:10.5194/acp-15-1707-2015, 2015.

Brioude, J., Petron, G., Frost, G. J., Ahmadov, R., Angevine, W. M., Hsie, E.-Y., Kim, S.-W., Lee, S.-H., McKeen, S. A., Trainer, M., Fehsenfeld, F. C., Holloway, J. S., Peischl, J., Ryerson, T. B., and Gurney, K. R.: A new inversion method to calculate emission inventories without a prior at mesoscale: Application to the anthropogenic CO_2 emission from Houston, Texas, J. Geophys. Res., 117, D05312, doi:10.1029/2011JD016918, 2012.

Broquet, G., Chevallier, F., Bréon, F.-M., Kadygrov, N., Alemanno, M., Apadula, F., Hammer, S., Haszpra, L., Meinhardt, F., Morguí, J. A., Necki, J., Piacentino, S., Ramonet, M., Schmidt, M., Thompson, R. L., Vermeulen, A. T., Yver, C., and Ciais, P.: Regional inversion of CO_2 ecosystem fluxes from atmospheric measurements: reliability of the uncertainty estimates, Atmos. Chem. Phys., 13, 9039–9056, doi:10.5194/acp-13-9039-2013, 2013.

Canadell, J. G., Le Quere, C., Raupach, M. R., Field, C. B., Buitenhuis, E. T., Ciais, P., Conway, T. J., Gillett, N. P., Houghton, R. A., and Marland, G.: Contributions to accelerating atmospheric CO_2 growth from economic activity, carbon intensity, and efficiency of natural sinks, P. Natl. Acad. Sci. USA, 104, 18866–18870, doi:10.1073/pnas.0702737104, 2007.

CDIAC: CDIAC emission inventory data, available at: http://cdiac.ornl.gov/trends/emis/tre_coun.html, last access: 28 October 2016.

Chevallier, F., Bréon, F.-M., and Rayner, P. J.: Contribution of the Orbiting Carbon Observatory to the estimation of CO_2 sources and sinks: Theoretical study in a variational data assimilation framework, J. Geophys. Res., 112, D09307, doi:10.1029/2006JD007375, 2007.

Chevallier, F., Ciais, P., Conway, T. J., Aalto, T., Anderson, B. E., Bousquet, P., Brunke, E. G., Ciattaglia, L., Esaki, Y., Fröhlich, M., Gomez, A., Gomez-Pelaez, A. J., Haszpra, L., Krummel, P. B., Langenfelds, R. L., Leuenberger, M., Machida, T., Maignan, F., Matsueda, H., Morguí, J. A., Mukai, H., Nakazawa, T., Peylin, P., Ramonet, M., Rivier, L., Sawa, Y., Schmidt, M., Steele, L. P., Vay, S. A., Vermeulen, A. T., Wofsy, S., and Worthy, D.: CO_2 surface fluxes at grid point scale estimated from a global 21 year reanalysis of atmospheric measurements, J. Geophys. Res., 115, D21307, doi:10.1029/2010JD013887, 2010.

Ciais, P., Dolman, A. J., Dargaville, R., Barrie, L., Bombelli, A., Butler, J., Canadell, P., and Moriyama, T.: Geo Carbon Strategy, Geo Secretariat Geneva, FAO, Rome, Italy, 48 pp., 2010a.

Ciais, P., Paris, J. D., Marland, G., Peylin, P., Piao, S. L., Levin, I., Pregger, T., Scholz, Y., Friedrich, R., Rivier, L., Houwelling, S., and Schulze, E. D.: The European carbon balance. Part 1: fossil fuel emissions. Glob. Change Biol., 16, 1395–1408, doi:10.1111/j.1365-2486.2009.02098.x, 2010b.

Ciais, P., Dolman, A. J., Bombelli, A., Duren, R., Peregon, A., Rayner, P. J., Miller, C., Gobron, N., Kinderman, G., Marland, G., Gruber, N., Chevallier, F., Andres, R. J., Balsamo, G., Bopp, L., Bréon, F.-M., Broquet, G., Dargaville, R., Battin, T. J., Borges, A., Bovensmann, H., Buchwitz, M., Butler, J., Canadell, J. G., Cook, R. B., DeFries, R., Engelen, R., Gurney, K. R., Heinze, C., Heimann, M., Held, A., Henry, M., Law, B., Luyssaert, S., Miller, J., Moriyama, T., Moulin, C., Myneni, R. B., Nussli, C., Obersteiner, M., Ojima, D., Pan, Y., Paris, J.-D., Piao, S. L., Poulter, B., Plummer, S., Quegan, S., Raymond, P., Reichstein, M., Rivier, L., Sabine, C., Schimel, D., Tarasova, O., Valentini, R., Wang, R., van der Werf, G., Wickland, D., Williams, M., and Zehner, C.: Current systematic carbon-cycle observations and the need for implementing a policy-relevant carbon observing system, Biogeosciences, 11, 3547–3602, doi:10.5194/bg-11-3547-2014, 2014.

Ciais, P., Crisp, D., van der Gon, H. D., Engelen, R., Janssens-Maenhout, G., Heimann M., Rayner P., and Scholze, M.: Towards a European Operational Observing System to Monitor Fossil CO_2 emissions, Final Report from the expert group, European Commission, Brussels, available at: http://www.copernicus.eu/main/ (last access: April 2016), 2015.

Clerbaux, C., Boynard, A., Clarisse, L., George, M., Hadji-Lazaro, J., Herbin, H., Hurtmans, D., Pommier, M., Razavi, A., Turquety, S., Wespes, C., and Coheur, P.-F.: Monitoring of atmospheric composition using the thermal infrared IASI/MetOp sounder, Atmos. Chem. Phys., 9, 6041–6054, doi:10.5194/acp-9-6041-2009, 2009.

Deming, W. E.: Sample design in business research, Wiley classics library ed., Wiley, New York, USA, 1990.

Ding, J., van der A, R. J., Mijling, B., Levelt, P. F., and Hao, N.: NO_x emission estimates during the 2014 Youth Olympic Games in Nanjing, Atmos. Chem. Phys., 15, 9399–9412, doi:10.5194/acp-15-9399-2015, 2015.

EC-JRC/PBL: Emission Database for Global Atmospheric Research (EDGAR), release version 4.2, available at: http://edgar.jrc.ec.europa.eu/overview.php?v=42 (last access: July 2015), 2011.

EMEP/CEIP: Present state of emission data, available at: http://www.ceip.at/ (last access: July 2015), 2014.

EMEP/EEA: EMEP/EEA Air Pollutant Emission Inventory Guidebook 2013, Technical report No. 12/2013, European Environment Agency, Copenhagen, Denmark, 2013.

Enting, I. G.: Inverse problems in atmospheric constituent transport, Cambridge University Press, Cambridge, New York, USA, 2002.

Eskes, H. J. and Boersma, K. F.: Averaging kernels for DOAS total-column satellite retrievals, Atmos. Chem. Phys., 3, 1285–1291, doi:10.5194/acp-3-1285-2003, 2003.

ESPRI: IASI CO retrievals, available at: http://ether.ipsl.jussieu.fr/ether/pubipsl/iasi_CO_uk.jsp, last access: 28 October 2016.

Folberth, G. A., Hauglustaine, D. A., Lathière, J., and Brocheton, F.: Interactive chemistry in the Laboratoire de Métorologie Dynamique general circulation model: model description and impact analysis of biogenic hydrocarbons on tropospheric chemistry, Atmos. Chem. Phys., 6, 2273–2319, doi:10.5194/acp-6-2273-2006, 2006.

Fortems-Cheiney, A., Chevallier, F., Pison, I., Bousquet, P., Carouge, C., Clerbaux, C., Coheur, P.-F., George, M., Hurtmans, D., and Szopa, S.: On the capability of IASI measurements to inform about CO surface emissions, Atmos. Chem. Phys., 9, 8735–8743, doi:10.5194/acp-9-8735-2009, 2009.

GCP: Ten Years of Advancing Knowledge on the Global Carbon Cycle and its Management (Authors: Lavinia Poruschi, Shobhakar Dhakal and Josep Canadell), Report No. 7, Tsukuba, available at: http://www.globalcarbonproject.org/ (last access: 30 April 2015), 2010.

GENEMIS (Generation of European Emission Data for Episodes) project: EUROTRAC Annual Report 1993, Part 5, EUROTRAC International Scientific Secretariat, Garmisch-Partenkirchen, Germany, 1994.

George, M., Clerbaux, C., Hurtmans, D., Turquety, S., Coheur, P.-F., Pommier, M., Hadji-Lazaro, J., Edwards, D. P., Worden, H., Luo, M., Rinsland, C., and McMillan, W.: Carbon monoxide distributions from the IASI/METOP mission: evaluation with other space-borne remote sensors, Atmos. Chem. Phys., 9, 8317–8330, doi:10.5194/acp-9-8317-2009, 2009.

Gregg, J. S., Andres, R. J., and Marland, G.: China: Emissions pattern of the world leader in CO_2 emissions from fossil fuel consumption and cement production, Geophys. Res. Lett., 35, L08806, doi:10.1029/2007GL032887, 2008.

Gu, D., Wang, Y., Smeltzer, C., and Boersma, K. F.: Anthropogenic emissions of NO_x over China: Reconciling the difference of inverse modeling results using GOME-2 and OMI measurements, J. Geophys. Res. Atmos., 119, 7732–7740, doi:10.1002/2014JD021644, 2014.

Guan, D., Liu, Z., Geng, Y., Lindner, S., and Hubacek, K.: The gigatonne gap in China's carbon dioxide inventories, Nat. Clim. Change, 2, 672–675, doi:10.1038/nclimate1560, 2012.

Guenther, A., Karl, T., Harley, P., Wiedinmyer, C., Palmer, P. I., and Geron, C.: Estimates of global terrestrial isoprene emissions using MEGAN (Model of Emissions of Gases and Aerosols from Nature), Atmos. Chem. Phys., 6, 3181–3210, doi:10.5194/acp-6-3181-2006, 2006.

Gurney, K. R., Law, R. M., Denning, A. S., Rayner, P. J., Baker, D., Bousquet, P., Bruhwiler, L., Chen, Y.-H., Ciais, P., Fan, S., Fung, I. Y., Gloor, M., Heimann, M., Higuchi, K., John, J., Maki, T., Maksyutov, S., Masarie, K., Peylin, P., Prather, M., Pak, B. C., Randerson, J., Sarmiento, J., Taguchi, S., Takahashi, T., and Yuen, C.-W.: Towards robust regional estimates of CO_2 sources and sinks using atmospheric transport models, Nature, 415, 626–630, doi:10.1038/415626a, 2002.

Gurney, K. R., Mendoza, D. L., Zhou, Y., Fischer, M. L., Miller, C. C., Geethakumar, S. and de la Rue du Can, S.: High Resolution Fossil Fuel Combustion CO_2 Emission Fluxes for the United States, Environ. Sci. Technol., 43, 5535–5541, doi:10.1021/es900806c, 2009.

Hooghiemstra, P. B., Krol, M. C., Bergamaschi, P., de Laat, A. T. J., van der Werf, G. R., Novelli, P. C., Deeter, M. N., Aben, I., and Röckmann, T.: Comparing optimized CO emission estimates using MOPITT or NOAA surface network observations, J. Geophys. Res., 117, D06309, doi:10.1029/2011JD017043, 2012.

Houweling, S., Breon, F.-M., Aben, I., Rödenbeck, C., Gloor, M., Heimann, M., and Ciais, P.: Inverse modeling of CO_2 sources and sinks using satellite data: a synthetic inter-comparison of measurement techniques and their performance as a function of space and time, Atmos. Chem. Phys., 4, 523–538, doi:10.5194/acp-4-523-2004, 2004.

Huang, C., Chen, C. H., Li, L., Cheng, Z., Wang, H. L., Huang, H. Y., Streets, D. G., Wang, Y. J., Zhang, G. F., and Chen, Y. R.: Emission inventory of anthropogenic air pollutants and VOC species in the Yangtze River Delta region, China, Atmos. Chem. Phys., 11, 4105–4120, doi:10.5194/acp-11-4105-2011, 2011.

Huneeus, N., Chevallier, F., and Boucher, O.: Estimating aerosol emissions by assimilating observed aerosol optical depth in a global aerosol model, Atmos. Chem. Phys., 12, 4585–4606, doi:10.5194/acp-12-4585-2012, 2012.

Hungershoefer, K., Breon, F.-M., Peylin, P., Chevallier, F., Rayner, P., Klonecki, A., Houweling, S., and Marshall, J.: Evaluation of various observing systems for the global monitoring of CO_2 surface fluxes, Atmos. Chem. Phys., 10, 10503–10520, doi:10.5194/acp-10-10503-2010, 2010.

Hurtmans, D., Coheur, P.-F., Wespes, C., Clarisse, L., Scharf, O., Clerbaux, C., Hadji-Lazaro, J., George, M., and Turquety, S.: FORLI radiative transfer and retrieval code for IASI, J. Quant. Spectrosc. Ra., 113, 1391–1408, doi:10.1016/j.jqsrt.2012.02.036, 2012.

IEA: CO_2 Emissions from Fuel Combustion 2010, OECD Publishing, Paris, France, doi:10.1787/9789264096134-en, 2010.

IPCC: 2006 IPCC Guidelines for National Greenhouse Gas Inventories, Prepared by the National Greenhouse Gas Inventories Programme, edited by: Eggleston, H. S., Buendia, L., Miwa, K., Ngara, T., and Tanabe, K., IGES, Japan, 2006.

IPCC: Summary for Policymakers. In: Climate Change 2013: The Physical Science Basis.Contribution of Working Group I to the Fifth Assessment Report of the Intergovernmental Panel on Climate Change, edited by: Stocker, T. F., Qin, D., Plattner, G.-K., Tignor, M., Allen S. K., Boschung, J., Nauels, A., Xia, Y., Bex, V., and Midgley, P. M., Cambridge University Press, Cambridge, UK and New York, NY, USA, 2013.

Janssens-Maenhout, G., Crippa, M., Guizzardi, D., Dentener, F., Muntean, M., Pouliot, G., Keating, T., Zhang, Q., Kurokawa, J., Wankmüller, R., Denier van der Gon, H., Kuenen, J. J. P., Klimont, Z., Frost, G., Darras, S., Koffi, B., and Li, M.: HTAP_v2.2: a mosaic of regional and global emission grid maps for 2008 and 2010 to study hemispheric transport of air pollution, Atmos. Chem. Phys., 15, 11411–11432, doi:10.5194/acp-15-11411-2015, 2015.

Jiang, Z., Jones, D. B. A., Worden, H. M., and Henze, D. K.: Sensitivity of top-down CO source estimates to the modeled vertical structure in atmospheric CO, Atmos. Chem. Phys., 15, 1521–1537, doi:10.5194/acp-15-1521-2015, 2015.

Kadygrov, N., Maksyutov, S., Eguchi, N., Aoki, T., Nakazawa, T., Yokota, T., and Inoue, G.: Role of simulated GOSAT total column CO_2 observations in surface CO_2 flux uncertainty reduction, J. Geophys. Res., 114, D21208, doi:10.1029/2008JD011597, 2009.

Kaiser, J. W., Heil, A., Andreae, M. O., Benedetti, A., Chubarova, N., Jones, L., Morcrette, J.-J., Razinger, M., Schultz, M. G., Suttie, M., and van der Werf, G. R.: Biomass burning emissions estimated with a global fire assimilation system based on observed fire radiative power, Biogeosciences, 9, 527–554, doi:10.5194/bg-9-527-2012, 2012.

Kaminski, T., Rayner, P. J., Heimann, M., and Enting, I. G.: On aggregation errors in atmospheric transport inversions, J. Geophys. Res., 106, 4703, doi:10.1029/2000jd900581, 2001.

Konovalov, I. B., Beekmann, M., Richter, A., and Burrows, J. P.: Inverse modelling of the spatial distribution of NO_x emissions on a continental scale using satellite data, Atmos. Chem. Phys., 6, 1747–1770, doi:10.5194/acp-6-1747-2006, 2006.

Konovalov, I. B., Beekmann, M., Burrows, J. P., and Richter, A.: Satellite measurement based estimates of decadal changes in European nitrogen oxides emissions, Atmos. Chem. Phys., 8, 2623–2641, doi:10.5194/acp-8-2623-2008, 2008.

Konovalov, I. B., Beekmann, M., Richter, A., Burrows, J. P., and Hilboll, A.: Multi-annual changes of NO_x emissions in megacity regions: nonlinear trend analysis of satellite measurement based estimates, Atmos. Chem. Phys., 10, 8481–8498, doi:10.5194/acp-10-8481-2010, 2010.

Konovalov, I. B., Beekmann, M., Kuznetsova, I. N., Yurova, A., and Zvyagintsev, A. M.: Atmospheric impacts of the 2010 Russian wildfires: integrating modelling and measurements of an extreme air pollution episode in the Moscow region, Atmos. Chem. Phys., 11, 10031–10056, doi:10.5194/acp-11-10031-2011, 2011.

Konovalov, I. B., Berezin, E. V., Ciais, P., Broquet, G., Beekmann, M., Hadji-Lazaro, J., Clerbaux, C., Andreae, M. O., Kaiser, J. W., and Schulze, E.-D.: Constraining CO_2 emissions from open biomass burning by satellite observations of co-emitted species: a method and its application to wildfires in Siberia, Atmos. Chem. Phys., 14, 10383–10410, doi:10.5194/acp-14-10383-2014, 2014.

Kopacz, M., Jacob, D. J., Fisher, J. A., Logan, J. A., Zhang, L., Megretskaia, I. A., Yantosca, R. M., Singh, K., Henze, D. K., Burrows, J. P., Buchwitz, M., Khlystova, I., McMillan, W. W., Gille, J. C., Edwards, D. P., Eldering, A., Thouret, V., and Nedelec, P.: Global estimates of CO sources with high resolution by adjoint inversion of multiple satellite datasets (MOPITT, AIRS, SCIAMACHY, TES), Atmos. Chem. Phys., 10, 855–876, doi:10.5194/acp-10-855-2010, 2010.

Korsbakken, J. I., Peters, G. P., and Andrew, R. M.: Uncertainties around reductions in China's coal use and CO_2 emissions, Nat. Clim. Change, 6, 687–690, doi:10.1038/nclimate2963, 2016.

Krol, M., Peters, W., Hooghiemstra, P., George, M., Clerbaux, C., Hurtmans, D., McInerney, D., Sedano, F., Bergamaschi, P., El Hajj, M., Kaiser, J. W., Fisher, D., Yershov, V., and Muller, J.-P.: How much CO was emitted by the 2010 fires around Moscow?, Atmos. Chem. Phys., 13, 4737–4747, doi:10.5194/acp-13-4737-2013, 2013.

Kurokawa, J., Ohara, T., Morikawa, T., Hanayama, S., Janssens-Maenhout, G., Fukui, T., Kawashima, K., and Akimoto, H.: Emissions of air pollutants and greenhouse gases over Asian regions during 2000–2008: Regional Emission inventory in ASia (REAS) version 2, Atmos. Chem. Phys., 13, 11019–11058, doi:10.5194/acp-13-11019-2013, 2013.

Lee, E. S. and Forthofer, R. N.: Analyzing complex survey data, 2nd ed., Sage Publications, Thousand Oaks, CA, USA, 2006.

Lehman, S. J., Miller, J. B., Wolak, C., Southon, J. R., Trans, P. P., Montzka, S. A., Sweeney, C., Andrews, A., LaFranchi, B., Guilderson, T. P., and Turnbull, J. C.: Allocation of terrestrial carbon sources using $^{14}CO_2$: Methods, measurement, and modeling, Radiocarbon, 55, 1484–1495, doi:10.2458/azu_js_rc.55.16392, 2013.

Levelt, P. F., Hilsenrath, E., Leppelmeier, G. W., van den Oord, G. H. J., Bhartia, P. K., Tamminen, J., de Haan, J. F., and Veefkind, J. P.: Science objectives of the ozone monitoring instrument, IEEE T. Geosci. Remote, 44, 1199–1208, doi:10.1109/TGRS.2006.872336, 2006.

Maksyutov, S., Takagi, H., Valsala, V. K., Saito, M., Oda, T., Saeki, T., Belikov, D. A., Saito, R., Ito, A., Yoshida, Y., Morino, I., Uchino, O., Andres, R. J., and Yokota, T.: Regional CO_2 flux estimates for 2009–2010 based on GOSAT and ground-based CO_2 observations, Atmos. Chem. Phys., 13, 9351-9373, doi:10.5194/acp-13-9351-2013, 2013.

Mareckova, K., Wankmueller, R., Moosmann, L., Pinterits, M., and Tisla, M.: Inventory Review 2007, Review of emission data reported under the LRTAP Convention and the NEC Directive, CEIP Technical Report 1/2014, Umweltbundesamt GmbH, Vienna, Austria, 2014.

Marland, G. and Rotty, R. M.: Carbon dioxide emissions from fossil fuels: a procedure for estimation and results for 1950–1982, Tellus B, 36, 232–261, doi:10.1111/j.1600-0889.1984.tb00245.x, 1984.

Martin, R. V., Jacob, D. J., Chance, K., Kurosu, T., Palmer, P. I., and Evans, M. J.: Global inventory of nitrogen oxide emissions constrained by space-based observations of NO_2 columns, J. Geophys. Res., 108, 4537, doi:10.1029/2003JD003453, 2003.

Menut, L., Bessagnet, B., Khvorostyanov, D., Beekmann, M., Blond, N., Colette, A., Coll, I., Curci, G., Foret, G., Hodzic, A., Mailler, S., Meleux, F., Monge, J.-L., Pison, I., Siour, G., Turquety, S., Valari, M., Vautard, R., and Vivanco, M. G.: CHIMERE 2013: a model for regional atmospheric composition modelling, Geosci. Model Dev., 6, 981–1028, doi:10.5194/gmd-6-981-2013, 2013.

Mijling, B. and van der A, R. J.: Using daily satellite observations to estimate emissions of short-lived air pollutants on a mesoscopic scale, J. Geophys. Res.-Atmos., 117, D17302, doi:10.1029/2012JD017817, 2012.

Miyazaki, K., Eskes, H. J., and Sudo, K.: Global NO_x emission estimates derived from an assimilation of OMI tropospheric NO_2 columns, Atmos. Chem. Phys., 12, 2263–2288, doi:10.5194/acp-12-2263-2012, 2012.

Miller, J. B., Lehman, S. J., Montzka, S. A., Sweeney, C., Miller, B. R., Karion, A., Wolak, C., Dlugokencky, E. J., Southon, J., Turnbull, J. C., and Tans, P. P.: Linking emissions of fossil fuel CO_2 and other anthropogenic trace gases using atmospheric $^{14}CO_2$, J. Geophys. Res., 117, D08302, doi:10.1029/2011JD017048, 2012.

Müller, J.-F. and Stavrakou, T.: Inversion of CO and NO_x emissions using the adjoint of the IMAGES model, Atmos. Chem. Phys., 5, 1157–1186, doi:10.5194/acp-5-1157-2005, 2005.

Napelenok, S. L., Pinder, R. W., Gilliland, A. B., and Martin, R. V.: A method for evaluating spatially-resolved NO_x emissions using Kalman filter inversion, direct sensitivities, and space-based NO_2 observations, Atmos. Chem. Phys., 8, 5603–5614, doi:10.5194/acp-8-5603-2008, 2008.

Nassar, R., Jones, D. B. A., Kulawik, S. S., Worden, J. R., Bowman, K. W., Andres, R. J., Suntharalingam, P., Chen, J. M., Brenninkmeijer, C. A. M., Schuck, T. J., Conway, T. J., and Worthy, D. E.: Inverse modeling of CO_2 sources and sinks using satellite observations of CO_2 from TES and surface flask measurements, Atmos. Chem. Phys., 11, 6029–6047, doi:10.5194/acp-11-6029-2011, 2011.

National Centers for Environmental Prediction: N. W. S., NOAA, U.S. Department of Commerce: NCEP/DOE Reanalysis 2 (R2), available at: http://rda.ucar.edu/datasets/ds091.0/ (last access: 9 September 2015), 2000.

Olivier, J. G. J., Van Aardenne, J. A., Dentener, F. J., Pagliari, V., Ganzeveld, L. N., and Peters, J. A. H. W.: Recent trends in global greenhouse gas emissions: regional trends 1970–2000 and spatial distributionof key sources in 2000, Environm. Sci., 2, 81–99, doi:10.1080/15693430500400345, 2005.

Palmer, P. I., Suntharalingam, P., Jones, D. B. A., Jacob, D. J., Streets, D. G., Fu, Q., Vay, S. A., and Sachse, G. W.: Using CO_2: CO correlations to improve inverse analyses of carbon fluxes, J. Geophys. Res., 111, D12318, doi:10.1029/2005JD006697, 2006.

Petit, J. R., Jouzel, J., Raynaud, D., Barkov, N. I., Barnola, J. M., Basile, I., Bender, M., Chappellaz, J., Davis, J., Delaygue, G., Delmotte, M., Kotlyakov, V. M., Legrand, M., Lipenkov, V., Lo-

rius, C., Pépin, L., Ritz, C., Saltzman, E., and Stievenard, M.: Climate and atmospheric history of the past 420,000 years from the Vostok Ice Core, Antarctica, Nature, 399, 429–436, 1999.

Pétron, G., Granier, C., Khattatov, B., Yudin, V., Lamarque, J. F., Emmons, L., Gille, J., and Edwards, D. P.: Monthly CO surface sources inventory based on the 2000–2001 MOPITT satellite data, Geophys. Res. Lett., 31, L21107, doi:10.1029/2004GL020560, 2004.

Press, W. H., Teukolsky, S. A., Vetterling, W. T., and Flannery, B. P.: Numerical Recipes in C: The Art of Scientific Computing (second edition). Cambridge University England Press, Cambridge, UK, 994 pp., ISBN 0-521-43108-5, 1992.

Politis, D. N., Romano, J. P., and Wolf, M.: Subsampling, Springer New York, New York, NY, USA, doi:10.1007/978-1-4612-1554-7, 1999.

Reuter, M., Buchwitz, M., Hilker, M., Heymann, J., Schneising, O., Pillai, D., Bovensmann, H., Burrows, J. P., Bösch, H., Parker, R., Butz, A., Hasekamp, O., O'Dell, C. W., Yoshida, Y., Gerbig, C., Nehrkorn, T., Deutscher, N. M., Warneke, T., Notholt, J., Hase, F., Kivi, R., Sussmann, R., Machida, T., Matsueda, H., and Sawa, Y.: Satellite-inferred European carbon sink larger than expected, Atmos. Chem. Phys., 14, 13739–13753, doi:10.5194/acp-14-13739-2014, 2014a.

Reuter, M., Buchwitz, M., Hilboll, A., Richter, A., Schneising, O., Hilker, M., Heymann, J., Bovensmann, H., and Burrows, J. P.: Decreasing emissions of NO_x relative to CO_2 in East Asia inferred from satellite observations, Nat. Geosci., 7, 792–795, doi:10.1038/ngeo2257, 2014b.

Rivier, L., Ciais, P., Hauglustaine, D. A., Bakwin, P., Bousquet, P., Peylin, P., and Klonecki, A.: Evaluation of SF_6, C_2Cl_4, and CO to approximate fossil fuel CO_2 in the Northern Hemisphere using a chemistry transport model, J. Geophys. Res., 111, D16311, doi:10.1029/2005JD006725, 2006.

Schmidt, H., Derognat, C., Vautard, R., and Beekmann, M.: A comparison of simulated and observed ozone mixing ratios for the summer of 1998 in Western Europe, Atmos. Environ., 35, 6277–6297, doi:10.1016/S1352-2310(01)00451-4, 2001.

Schoeberl, M. R., Douglass, A. R., Hilsenrath, E., Bhartia, P. K., Beer, R., Waters, J. W., Gunson, M. R., Froidevaux, L., Gille, J. C., Barnett, J. J., Levelt, P. F., and DeCola, P.: Overview of the EOS aura mission, IEEE T. Geosci. Remote, 44, 1066–1074, doi:10.1109/TGRS.2005.861950, 2006.

Schulze, E.-D., Luyssaert, S., Ciais, P., Freibauer, A., Janssens, I. A., Soussana, J. F., Smith, P., Grace, J., Levin, I., Thiruchittampalam, B., Heimann, M., Dolman, A. J., Valentini, R., Bousquet, P., Peylin, P., Peters, W., Rödenbeck, C., Etiope, G., Vuichard, N., Wattenbach, M., Nabuurs, G. J., Poussi, Z., Nieschulze, J., Gash, J. H., and the CarboEurope Team: Importance of methane and nitrous oxide for Europe's terrestrial greenhouse gas balance, Nat. Geosci., 2, 842–850, 2009.

Seinfeld, J. H. and Pandis, S. N.: Chemistry of the troposphere. In Atmospheric chemistry and physics: From air pollution to climate change, 2nd ed., Wiley-Interscience, J. Wiley & Sons, Inc, New York, USA, 204–230, 2006.

Silva, S. J., Arellano A. F., and Worden H.: Toward anthropogenic combustion emission constraints from space-based analysis of urban CO_2 / CO sensitivity, Geophys. Res. Lett., 40, 4971–4976, doi:10.1002/grl.50954, 2013.

Skamarock, W. C., Klemp, J. B., Dudhia, J., Gill, D. O., Barker, D. M., Duda, M. G., Huang, X.-Y., Wang W., and Powers, J. G.: A Description of the advanced research WRF version 3, NCAR Tech. Note, NCAR/TN-475+STR, Boulder, Colorado, USA, 113 pp., 2008.

Stohl, A., Williams, E., Wotawa, G., and Kromp-Kolb, H.: A European inventory of soil nitric oxide emissions and the effect of these emissions on the photochemical formation of ozone in Europe, Atmos. Environ., 30, 3741–3755, 1996.

Suntharalingam, P., Jacob, D. J., Palmer, P. I., Logan, J. A., Yantosca, R. M., Xiao, Y., Evans, M. J. Streets, D. G., Vay, S. L., and Sachse, G. W.: Improved quantification of Chinese carbon fluxes using CO_2 / CO correlations in Asian outflow, J. Geophys. Res., 109, D18S18, doi:10.1029/2003JD004362, 2004.

Tarassón, L., Jonson, J. E., Berntsen, T. K., and Rypdal, K.: Study on air quality impacts of non-LTO emissions from aviation, Final report to the European Commission under contract B4-3040/2002/343093/MAR/C1, CICERO, Oslo, available at: http://ec.europa.eu/environment/air/pdf/air_quality_impacts_finalreport.pdf (last access: October 2016), 2004.

TEMIS: OMI retrievals, available at: http://www.temis.nl/, last access: 28 October 2016.

Turnbull, J., Rayner, P., Miller, J., Naegler, T., Ciais, P., and Cozic, A.: On the use of $^{14}CO_2$ as a tracer for fossil fuel CO_2: Quantifying uncertainties using an atmospheric transport model, J. Geophys. Res., 114, D22302, doi:10.1029/2009JD012308, 2009.

Turquety, S., Hurtmans, D., Hadji-Lazaro, J., Coheur, P.-F., Clerbaux, C., Josset, D., and Tsamalis, C.: Tracking the emission and transport of pollution from wildfires using the IASI CO retrievals: analysis of the summer 2007 Greek fires, Atmos. Chem. Phys., 9, 4897–4913, doi:10.5194/acp-9-4897-2009, 2009.

UN: Energy Statistics Yearbook, United Nations Department for Economic and Social Information and Policy Analysis, Statistics Division, New York, USA, 2012.

UNFCCC: Kyoto Protocol to the United Nations Framework Convention on Climate Change, United Nations, available at: http://unfccc.int/resource/docs/convkp/kpeng.pdf (last access: October 2016), 1998.

UNFCCC: Paris Agreement to the United Nations Framework Convention on Climate Change, United Nations, available at: https://unfccc.int/resource/docs/2015/cop21/eng/l09r01.pdf (last access: October 2016), 2015.

Vinken, G. C. M., Boersma, K. F., Maasakkers, J. D., Adon, M., and Martin, R. V.: Worldwide biogenic soil NO_x emissions inferred from OMI NO_2 observations, Atmos. Chem. Phys., 14, 10363–10381, doi:10.5194/acp-14-10363-2014, 2014.

Wang, R., Tao, S., Ciais, P., Shen, H. Z., Huang, Y., Chen, H., Shen, G. F., Wang, B., Li, W., Zhang, Y. Y., Lu, Y., Zhu, D., Chen, Y. C., Liu, X. P., Wang, W. T., Wang, X. L., Liu, W. X., Li, B. G., and Piao, S. L.: High-resolution mapping of combustion processes and implications for CO_2 emissions, Atmos. Chem. Phys., 13, 5189–5203, doi:10.5194/acp-13-5189-2013, 2013.

Zhao, B., Wang, P., Ma, J. Z., Zhu, S., Pozzer, A., and Li, W.: A high-resolution emission inventory of primary pollutants for the Huabei region, China, Atmos. Chem. Phys., 12, 481–501, doi:10.5194/acp-12-481-2012, 2012..

Zhao, C. and Wang, Y.: Assimilated inversion of NO_x emissions over east Asia using OMI NO_2 column measurements, Geophys. Res. Lett., 36, L06805, doi:10.1029/2008GL037123, 2009.